Geophys. J. Int. (2001) **146,** 850–866

Cretaceous–Tertiary geodynamics: a North Atlantic exercise

Trond H. Torsvik,[1,2] Jon Mosar[1] and Elizabeth A. Eide[1]

[1] *Geological Survey of Norway, Leiv Eirikssons vei* 39, N-7491 *Trondheim, Norway. Email: trond.torsvik@ngu.no*
[2] *Department of Mineralogy and Petrology, Lund University, Sölveg.* 13, S-223 62, *Sweden.*

Accepted 2001 May 10. Received 2000 September 11; in original form 2000 February 15

SUMMARY

New reconstructions are presented for the Cretaceous–Early Tertiary North Atlantic using a combination of palaeomagnetic, hotspot and magnetic anomaly data. We utilize these reconstructions in an analysis of previously described misfits between the North Atlantic Plate elements at successive intervals during this time period. We are able to achieve reasonable overlap between the hotspot and palaeomagnetic reconstructions between 40 and 95 Ma and thus are able to support the idea that the Indo–Atlantic hotspots are relatively stationary. Small, but systematic discrepancies for this time interval can readily be modelled with a long-term, octopole non-dipole field contribution ($G3 = g_3^0/g_1^0 = 0.08$). However, hotspot and palaeomagnetic reconstructions for the Early Cretaceous North Atlantic show substantial differences that cannot be explained by constant, non-dipole fields and we favour an explanation for these discrepancies in terms of true polar wander (TPW) triggered by mantle instabilities between 125 and 95 Ma; this constitutes the only identifiable event of significant TPW since the Early Cretaceous. Taken in the context of available geochronological and geological data and seismic tomography from the region, the 95–40 Ma reconstructions and their time-consequent geological products are interpreted in terms of specific conditions of mantle-crust coupling and global plate motions/tectonic activity. Highlights from these reconstructions show uniform NE movement of the coupled North American, Greenland and Eurasian plates from 95 to 80 Ma; a marked cusp in the paths for all three elements at 80 Ma where the three plates simultaneously change direction and follow a uniform NW-directed motion until *c*. 20 Ma when Eurasia diverges NE, away from the still-NW-moving Greenland and North American elements. Positioning of the Iceland plume beneath the spreading-ridge at 20 Ma may have increased upwelling below the ridge, increased the ridge-push, and caused a NE shift in the absolute direction of Eurasia.

Key words: geodynamics, hotspots, Iceland plume, non-dipole field, palaeomagnetism, plate reconstructions, true polar wander.

1 INTRODUCTION

Magnetic anomaly data, globally applicable from mid-Jurassic times, provide relative fits between continents, whilst palaeomagnetic data yield palaeolatitudinal and rotational constraints for continents throughout geological history. Additionally, from the Early Cretaceous onward, hotspot reconstructions offer a unique contribution to palaeoreconstructions since they provide palaeolongitudinal control for plate positions, a feature otherwise absent in palaeomagnetic data. A fundamental assumption with hotspot reconstructions is that the hotspots are stationary, or move at insignificant speeds, relative to plate-tectonic velocities. Hotspot and palaeomagnetic data can thus provide independent reference schemes to make plate reconstructions such that discrepancies between two palaeoreconstructions each derived, respectively, from these data sets, can be utilized to evaluate the initial data quality and the accuracy of the reconstructions themselves. Discrepancies between the two data sets (i.e. a misfit between two palaeoreconstructions) are most commonly explained by invoking true polar wander (TPW), driven by changes in the Earth's moment of inertia (e.g. Jurdy 1981; Gordon 1987; Besse & Courtillot 1991; Van Fossen & Kent 1992; Prévot *et al*. 2000), or by inferring that hotspots are not as stationary as assumed (e.g. Norton 1995; Tarduno & Cottrell 1997; Steinberger & O'Connell 1998).

The North Atlantic is a classic area in which to address palaeoreconstructions and related issues like continental break-up and seafloor spreading, rift propagation, mantle plumes and

magmatic processes. In this vein, several critical reconstruction studies for the North Atlantic region have generated better knowledge of the general dynamics of ocean opening relative to factors like plume arrival, the specifics of timing and style of magma emplacement before and during break-up, and the relative motion of continents (e.g. Srivastava & Roest 1989; Roest & Srivastava 1989; Rowley & Pindell 1989; Lottes & Rowley 1990; Lawver & Müller 1994). Magnetic anomaly fits have been used extensively for these North Atlantic reconstructions beginning with anomaly A33 (*c.* 80 Ma) which, according to Roest & Srivastava (1989), is the oldest identified magnetic anomaly in the region (in the Labrador Sea between Greenland and North America). In this account we examine Cretaceous–Early Tertiary reconstructions focusing on the North Atlantic and explore the geodynamic evolution in this area for the last 130 Myr using combined palaeomagnetic, hotspot and magnetic anomaly data. The reconstructions allow us to test for conceivable discrepancies in the palaeomagnetic and hotspot reference frame and subsequently to use these results to generate reconstructions that comply with subsurface geological data and global plate motions.

2 BACKGROUND

The North Atlantic Igneous Province (NAIP), includes the UK, Ireland, the Faeroes, Greenland and the West Greenland–Baffin corridor (Fig. 1), and is one of several well-known flood-basalt provinces (e.g. Deccan & Parana Traps, Courtillot *et al.* 1999) temporally correlated with continental break up. In the NAIP, the various volcanic regions have been linked to the Iceland plume and broadly correspond in time to the initiation of seafloor spreading in the NE Atlantic. Anomaly 24 (52.364–53.347 Ma, Cande & Kent 1995) is the oldest normal polarity chron identified in the NE Atlantic, but seafloor spreading might had already begun during the preceding reverse polarity chron (A24r), thus an absolute maximum age for initiation of seafloor spreading would be 55.9 Ma, i.e. Late Palaeocene epoch (Late Thanetian age). The NAIP itself, excluding the youngest Icelandic rocks, shows a wide age-range (*c.* 20–64 Ma, see Fig. 2 and discussion below), but based on isotope data from Greenland, Tegner & Duncan (1999) and Tegner *et al.* (1998) have identified discrete episodes of pre- (~63–59 Ma), syn- (~57–54 Ma) and post- (~50 Ma) break

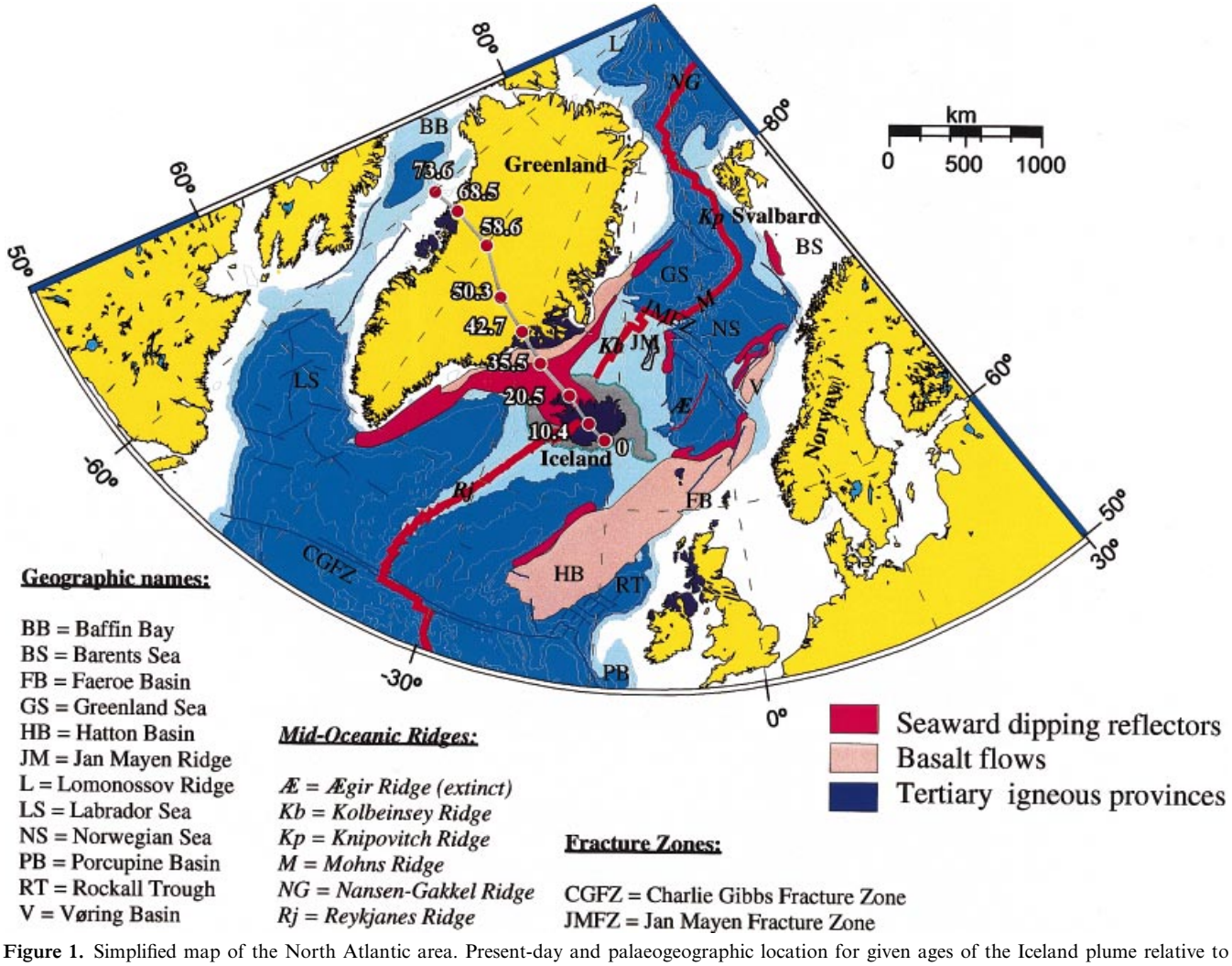

Figure 1. Simplified map of the North Atlantic area. Present-day and palaeogeographic location for given ages of the Iceland plume relative to Greenland assuming that the plume is fixed in the mantle (hotspot frame). Igneous provinces, basalt flows, seaward dipping reflectors, mid-ocean ridges and major transform faults are shown.

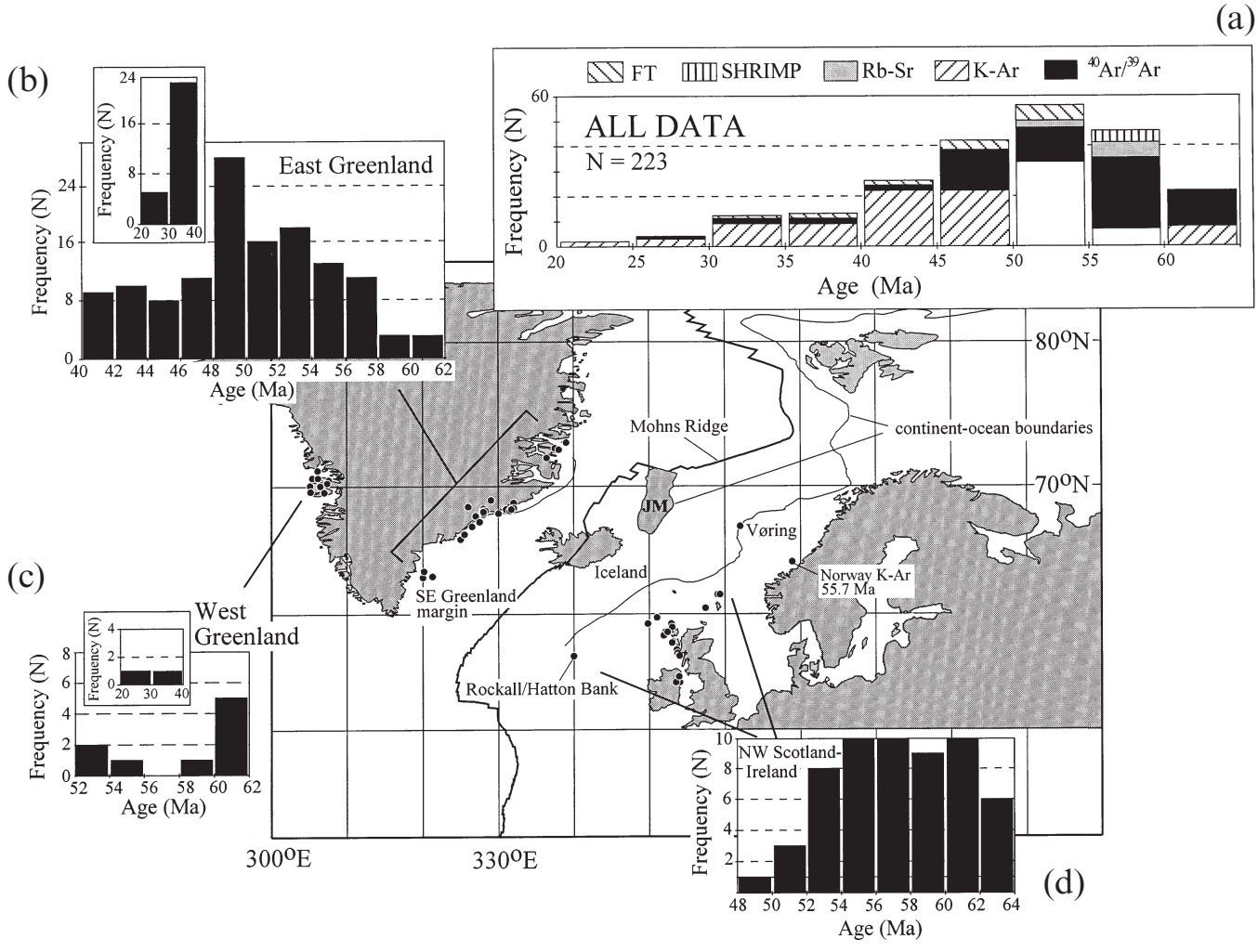

Figure 2. Frequency distributions of published, fully documented isotopic age data from the North Atlantic Igneous Province with sample locations; note that more than 220 data-points are plotted on the map and that sample points at this scale often overlap. Data were compiled and analysed with the NGU Isotope Database (Torsvik & Eide 1998); the data table for this diagram with the complete set of references can be found in the Appendix. Age uncertainties are given at 2 σ. (a) All reliable ages from the NAIP separated in 5 my. time windows and separated into isotope analytical method. Because these data are naturally biased (see text for discussion), no significance can be attributed to the apparent 'peak' in ages between 50 and 55 Ma. Geographical breakdown of the same data set (b-d) is slightly more useful to deduce general age patterns that can then be linked to palaeoreconstructions; data in (b)–(d) are not separated by isotope method. (b) East Greenland and offshore East Greenland age data; inset shows the smaller population of younger ages from the region. (c) West Greenland age data (onshore) with inset of the two younger ages obtained in the region (see text).(d) NW Scotland-Ireland and offshore British sector age data. The single point from the margin of Norway is noted on the map.

up related volcanism on the East Greenland margin. The pre-break up melting event is assumed to have been triggered by arrival of the Icelandic plume under Central Greenland (Fig. 1), associated with production of primitive, very high-temperature magmas at dispersed localities around the North Atlantic province (West and South-east Greenland, the Inner Hebrides and NE Ireland).

The synthetic hotspot track for the Iceland hotspot (relative to Greenland) in Fig. 1 assumes a stationary hotspot, presently located at 64°N and 16°W, and was calculated from the hotspot model of Müller *et al.* (1993) and magnetic anomaly fits. This track is quite similar to that of Lawver & Müller (1994) and implies that the Iceland hotspot was located beneath West-Central Greenland at *c.* 60 Ma and subsequently at the East Greenland Margin at *c.* 40 Ma (Fig. 1). This observation, if correct, led Lawver & Müller (1994) to argue that Early Tertiary volcanism along the North Atlantic margins reflected rifting of already thinned crust rather than the arrival of a single plume head that itself instigated all rifting and volcanism. This topic of the Iceland plume shape as related to the style and timing of initial volcanism in the North Atlantic remains a point of discussion but does not affect the reconstructions presented in this study—data from the Iceland plume are never used as direct input for the reconstructions. Our reconstructions instead can be used in the reverse sense; to constrain the movement of plates over the plume during the Cenozoic and the extent of Iceland plume volcanism for specific time intervals.

3 NORTH ATLANTIC VOLCANIC PROVINCE: TERTIARY AGE SUMMARY

A brief review of published isotope geochronological data for Palaeogene volcanic rocks distributed around the North Atlantic is useful to link plume magmatism to the plate motions

pertaining to our reconstructions. The published geochronological data comprise more than 220 reliable ages (from a total of more than 270) from East and West Greenland, Scotland, Ireland and offshore regions (Fig. 2; Appendix). Most of the data (*c*. 70 per cent) are derived from East Greenland (see Summary in Tegner *et al*. 1998) with 29 per cent from NW Scotland and Ireland and their offshore counterparts; the small remainder are derived from one study in West Greenland (Storey *et al*. 1998) and one data point from the West Norway margin. The majority of the ages are from K–Ar (>50 per cent) or $^{40}Ar/^{39}Ar$ data (*c*. 36 per cent), with a limited subset from Rb–Sr, SHRIMP (zircon) and fission track (FT) (zircon, titanite and apatite) data. A simple frequency diagram of all reliable ages (Fig. 2a), filtered to remove those ages determined clearly to represent post-emplacement cooling (rather than crystallization), shows a data peak between 50 and 55 Ma. The geological significance of this peak is muted by inherent bias in the combined data set that include: (1) logistical and accessibility limitations that have left a large volume of NAIP material unsampled (2) over-sampling (multiple dating) of some outcrops, flows or complexes. While age-data of the latter type are often very reliable, their presence in the data set is not readily distinguished based on literature descriptions alone and thus their influence on age distributions is difficult to assess. Several approaches to overcome some of this bias have been previously taken (e.g. combining detailed geochemical analyses with geochronology and rock type, see Saunders *et al*. 1997; Tegner *et al*. 1998). Here we attempt to extract more meaningful information from these data in Fig. 2(b–d) by organising the data according to specific sampling region (geography) and within smaller time windows (2 Myr age bins).

In Fig. 2(b), the East Greenland data set reveals magmatic activity throughout the entire Palaeogene with a dominant age group between 48 and 50 Ma and a subsidiary peak between 52 and 54 Ma (the inset with ages <40 Ma is not discussed further). The East Greenland data set also incorporates some offshore points from the SE Greenland margin and one datapoint from the Vøring plateau that yield ages, respectively, of 59.4, 60.3, 61.0, 62.3, and 63.3 Ma (SE Greenland boreholes) and 54.3 Ma (Vøring) (see study by Sinton & Duncan 1998). The West Greenland data (Fig. 2c), while more restricted in total number, span from 52 to 62 Ma with an apparent data peak between 60 and 62 Ma and a age gap between 56 and 58 Ma; two late Palaeogene ages (27.4 Ma and 34.1 Ma, from an alkaline basalt and a lamprophyre dyke, respectively) are also reported (see inset, Fig. 2c and Storey *et al*. 1998). In the NW Scotland–Ireland data set, published ages range between 48 and 64 Ma with no obvious age peak. No younger Palaeogene ages have been reported from the region. The near and far-offshore core data are clustered around N and NW Scotland (near Shetland, the Hebrides and Rosemary Bank; Hitchen & Ritchie 1993), with one data point from the Rockall/Hatton Bank region (51.6 Ma; Sinton & Duncan 1998) (see also Fig. 2). A single K–Ar age of 55.7 ± 0.9 Ma (2 σ) from a grab sample in a shallow offshore core near Kristiansund, Norway, may demarcate the eastward extent of Tertiary volcanic activity in the North Atlantic region (Bugge *et al*. 1980).

Several general patterns can be reliably extracted from these geographical data groupings. First, each of the areas shows evidence for early Palaeocene (>60 Ma) magmatism, coincident with the drift period in the Labrador Sea and the pre-drift period in the North Atlantic (see also Saunders *et al*. 1997). Second, the extent of magmatic activity, well into the Oligocene on both East and West Greenland, indicates prolonged magmatic activity on both margins. Furthermore, while the lack of younger (Oligocene) ages in the NW Scotland–Ireland region could be attributed to a sampling bias (unsampled rocks offshore), it may just as likely reflect a shift of magmatic activity away from this region at a specific time interval. These patterns are discussed further below in the context of the palaeoreconstructions.

4 COMPARISON OF HOTSPOT AND PALAEOMAGNETIC RECONSTRUCTIONS

Based on volcanic hotspot tracks from the North American, South American, African, and Indian-Australian Plates, Müller *et al*. (1993) estimated best-fit plate rotations relative to present-day hotspots since the Early Cretaceous (M10, *c*. 130 Ma). Their internally consistent plate-motion model implies no relative motion between hotspots for the past 84 Ma, but the model has inherent geometric ($\pm$220–275 km in latitude) and age uncertainties. The older part of the model is subject to the largest uncertainties since it is based on tracks from only the Tristan da Cunha (South Atlantic) and Great Meteor (Central Atlantic) hotspots. The latter produced the New England Seamounts that provide a trail for the North American plate.

Recent studies from the Pacific Ocean cast doubts on stationary hotspots and Tarduno & Cottrell (1997) have suggested that the Hawaii hotspot has moved southwards at speeds of *c*. 3 cm yr^{-1}. The global mantle circulation model (Steinberger & O'Connell 1998; Steinberger 2000) also predicts considerable hotspot migration rates. In order to test for discrepancies between the palaeomagnetic and hotspot frames, we undertook a detailed comparison of the two data sets for the North Atlantic region. Our palaeomagnetic analysis uses Cretaceous–Early Tertiary palaeopoles from North America and Europe (Torsvik *et al*. 2001). The North American and European continents were reconstructed on the basis of magnetic anomalies and estimates of pre-drift extension as explained by Torsvik *et al*. (2001). After rotation according to the reconstructions, mean palaeopoles were calculated with a 20 Myr moving window at 5 Ma increments (Table 1; North America coordinates).

In order to associate the mean poles with respect to the North America hotspot reference we rotated the palaeomagnetic poles according to the hotspot frame of Müller *et al*. (1993), but used interpolated rotation poles to match the mean age of individual palaeomagnetic poles. Ideally, the rotated palaeomagnetic poles should thus fall at the north pole if the palaeomagnetic and hotspot frames are identical (Fig. 3a).

Fig. 3 shows a reasonable match in Late Cretaceous and Early Tertiary times [1.4–6.9° angular deviation (AD), i.e. great circle angle between the palaeomagnetic pole and 90°N], but from 100 Ma and older time periods, major deviations are observed and amount to a high of 21° at 130 Ma.

4.1 True polar wander in the Early Cretaceous

The Indo–Atlantic hotspot analysis of Prévot *et al*. (2000) (Fig. 3d) yields similar results to our own analysis (see comparison in Fig. 3b). Both data sets indicate a sharp drop in AD during the 125 and 95 Ma interval that must be accounted for

Table 1. Palaeomagnetic poles for North America and Eurasia combined (North American co-ordinates; Torsvik *et al.* 2001), and calculated poles with respect to the hotspot frame (Müller *et al.* 1993). Poles are listed for a geocentric axial dipole (GAD), and for an optimized model (40–95 Ma range; see text) that assumes an axial geocentric dipole and an octupole ($G3 = g_3^\circ/g_1^\circ = 0.08$). A95 = 95 per cent confidence circle around the mean pole; Lat. = Latitude; Long. = Longitude; AD = angular deviation (great-circle distance in degrees) between the palaeomagnetic and hotspot frame.

Age ±10 Ma	GAD Model					8 per cent octupole Model					AD
	A95	Pole		Hotspot referenced		A95	Pole		Hotspot referenced		
		Lat.	Long.	Lat.	Long.		Lat.	Long.	Lat.	Long.	
40	5.3	82.1	167.6	85.8	135.3	4.8	82.7	206.3	87.8	234.3	2.2
45	3.4	80.6	162.1	84.4	128.1	3.0	82.9	194.7	89.3	175.9	0.7
50	2.9	77.8	169.5	83.4	143.5	2.8	80.6	190.8	87.9	168.5	2.1
55	2.5	77.1	172.9	83.6	143.9	2.5	79.4	193.8	88.0	176.5	2.0
60	2.7	75.8	174.3	83.2	143.0	2.7	78.5	191.9	87.9	153.6	2.1
65	2.8	73.6	179.8	83.0	153.8	3.0	75.8	194.2	87.0	175.2	3.0
70	4.1	73.7	189.5	85.4	164.4	4.1	73.0	206.3	86.0	232.8	4.0
75	6.2	71.7	194.8	85.4	194.7	6.4	70.7	208.9	84.2	245.7	5.8
80	5.4	72.3	184.8	85.4	163.2	6.5	73.9	196.8	88.5	213.6	1.5
85	6.2	72.5	184.1	87.1	178.5	7.5	75.1	196.6	88.1	304.8	1.9
90	4.9	73.6	180.3	88.6	181.3	6.6	77.3	192.2	86.7	346.8	3.3
95	5.2	73.6	170.5	87.9	167.9	6.8	78.5	179.3	86.6	004.2	3.4
100	8.1	74.6	182.1	85.6	278.4	8.6	77.1	205.6	80.6	311.5	9.4
105	5.1	75.6	186.2	82.9	294.2	5.6	76.4	214.3	76.7	310.5	13.2
110	4.6	75.5	189.5	80.1	295.5	4.9	76.1	218.0	73.9	310.1	16.1
115	3.2	72.9	194.3	75.6	288.0	3.1	73.9	219.3	70.3	304.9	19.6
120	3.2	72.4	196.6	72.4	289.6	2.9	73.6	220.5	67.5	304.7	22.4
125	4.1	71.1	198.2	69.9	289.1	3.6	72.5	220.7	65.4	303.9	24.6
130	3.7	71.0	196.3	68.9	289.8	3.7	73.0	217.7	65.0	304.2	25.0

by a *c.* 20° tilt in the Earth's rotation axis in the Lower Cretaceous; such a dramatic tilt implicates TPW. Prévot *et al.* (2000) argued for relatively 'instantaneous' tilting at *c.* 110 Ma (5° Ma^{-1}). Our data appear to support a more protracted TPW event between 125 and 95 Ma but obviously a moving window will smooth the record; we tested this issue by generating mean palaeopoles with different moving window lengths and increment values (including non-overlapping mean poles), as well as by calculating mean poles with spherical spline methods (Torsvik *et al.* 1996). In all cases we observe a smooth transition between 125 and 95 Ma.

Prévot *et al.* (2000) pointed out that the TPW implied by the large change in AD must have occurred within the Cretaceous Normal Superchron (CNS; *c.* 118–84 Ma; Cande & Kent 1995). Superchrons document protracted time periods when the Earth's magnetic field did not change polarity and the Late Palaeozoic and Mesozoic contain two magnetic polarity Superchrons, i.e. the CNS and the Kiaman Reverse Superchron (KRS; *c.* 311–262 Ma) (McElhinny 1971; Courtillot & Besse 1987; Johnson *et al.* 1995; Eide & Torsvik 1996; Opdyke & Channell 1996). Various explanations have attempted to clarify the origin of Superchrons, which have causal elements within the Earth's outer core and lower mantle, by linking the complex and sometimes enigmatic cause-and-effect relationships between the Earth's core, mantle and crust. In the case of the CNS, mantle studies have led to suggested temporal links between the initiation of this superchron and relatively contemporaneous phenomena of TPW, continental break up, mantle plumes and anomalously high surface volcanic production (Courtillot & Besse 1987; Larson & Olson 1991). Conversely, Eide & Torsvik (1996) proposed catastrophic mantle flushing as the main element behind onset of the late Palaeozoic KRS; a similar explanation has been applied as an alternative explanation for the CNS (Gallet & Hulot 1997). Because mantle instabilities are likely candidates to trigger shifts in the Earth's pole of rotation (Weinstein 1993), lower mantle thermal anomalies have been related to periods of enhanced TPW (Gurnis & Torsvik 1994). As both Superchrons and TPW are grounded in fundamental ways to thermal anomalies in the lower mantle and the CNS is temporally linked to a major TPW event, we raise the possibility of a causal relationship between Superchrons and TPW.

4.2 Non-dipole fields

Considering the statistical errors in both the palaeomagnetic and hotspot analyses, it is somewhat premature to evaluate the significance of the minor angular deviations (*c.* 5° average) in the Late Cretaceous–Tertiary record (Fig. 3b). We do notice, however, that the Late Cretaceous–Tertiary mean poles are not centred around the North Pole [95–40 Ma poles in our analysis (Fig. 3a) and 0–80 Ma poles (Fig. 3d) of Prévot *et al.* 2000)], and systematically plot at lower latitudes at around 150°E.

Palaeomagnetic results rely on the fundamental hypothesis that the time-averaged geomagnetic field is that of a geocentric axial dipole (GAD), and palaeomagnetic poles are therefore assumed to coincide with the palaeogeographic poles. However, palaeomagnetic poles determined for the last five million years demonstrate that the time-averaged field deviates from that of a pure GAD McElhinny *et al.* (1996) estimated non-dipole quadrupole ($G2 = g_2^0/g_3^0$) and octupole ($G3 = g_3^0/g_1^0$) fields in the order of 3–9 per cent. Resolution of the differences in the palaeomagnetic and hotspot frames (e.g. Besse & Courtillot 1991; Van Fossen & Kent 1992; Prévot *et al.* 2000) has been

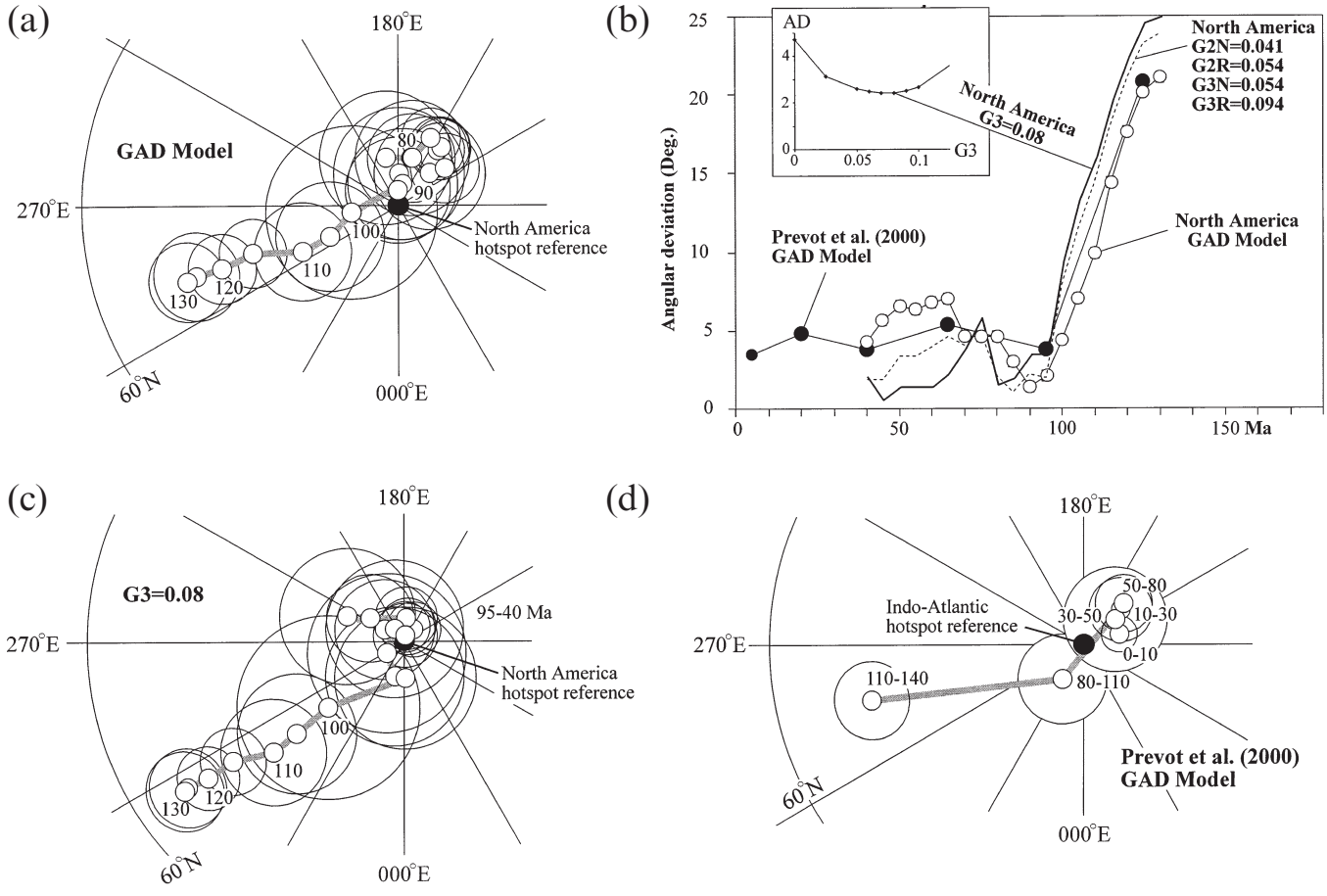

Figure 3. (a) Palaeomagnetic mean poles and A95 confidence circles for North America-Eurasia (Table 1) with respect to the hotspot frame (Müller *et al.* 1993), i.e. 90°N in the diagram (equal area polar projection). GAD model. (b) Calculated angular deviation (AD) between the hotspot and palaeomagnetic frames. North America GAD model (open circles), 8 per cent octupole model (solid line) and a more complex field model (McElhinny *et al.* 1996) based on the time-averaged field for the last five million years (both G2 & G3 contributions; N/R = normal/reverse polarity) are calculated from present study (see text for details). Results from Prévot *et al.* (2000) is plotted as solid circles. Inset diagram shows the variation in AD with increasing values of G3 (pure octupole models). (c) As (a) but with palaeomagnetic mean poles based on an 8 per cent octupole field contribution. (d) Mean palaeomagnetic poles calculated by Prévot *et al.* (2000) with reference to the Indo-Atlantic hotspot reference.

attempted by applying quadrupole models, but these efforts have met with limited success. Van der Voo & Torsvik (2001) suggest that long-term quadrupole fields are less likely than octupole fields and have estimated a long-term non-dipole octupole field of 10 per cent (G3 = 0.1) in Late Palaeozoic to Early Tertiary times.

In Fig. 3(c) we plot palaeomagnetic mean poles with respect to the hotspot frame (as Fig. 3a), but original palaeomagnetic data and mean poles were recalculated with an 8 per cent non-dipole octupole field. It is now evident that 95–40 Ma mean poles centre at the hotspot reference (90°N), and an average AD of $4.7 \pm 1.9°$ (1σ error), based on the GAD model (95–40 Ma poles), is reduced by almost 50 per cent (i.e. to $2.6 \pm 1.3°$). The 5–10 per cent octupole fields produce reasonable fits (statistically similar) but with 8 per cent as the best fit (Fig. 3b). We therefore argue that long-term octupole fields successfully eliminate small but systematic Late Cretaceous–Tertiary discrepancies in the palaeomagnetic and hotspot frames; in simple terms, a positive G3 leads to an underestimate of the palaeolatitude, and at a mid-latitude (50°N/S) this results in a 6.1° error in the palaeolatitude.

It is also possible to achieve a good fit between the palaeomagnetic and hotspot frame with much more complex geomagnetic field models. As an example, G2 and G3 values for the time-averaged field over the past 5 million years for continental data (McElhinny *et al.* 1996) produce a reasonably good fit with AD of $2.91 \pm 1.26°$ (Fig. 3b). This model also incorporates different G2 and G3 values for normal and reverse fields.

The Early Cretaceous differences we observe in the palaeomagnetic and hotspot frames would require large (25 per cent), non-uniform, and *negative* G3 values, the combination of which is geophysically unlikely. Thus, we find the most straightforward explanation for the deviations observed between these reference frames to be that of TPW in the Early Cretaceous. This explanation renders Early Cretaceous plate reconstructions for the North Atlantic undefensible and the palaeoreconstructions discussed subsequently are therefore restricted to Late Cretaceous–Tertiary times. With an 8 per cent octupole non-dipole field model, TPW amounts to 22–25° (130–125 Ma), whereas the rate of TPW approximates 0.75°/Ma (125–95 Ma). In contrast to some earlier analyses of TPW (e.g. Besse & Courtillot 1991) it is very important to note that the analyses of Prévot *et al.* (2000) and our own demonstrate only one significant event of TPW since the Early Cretaceous (assuming that the hotspot frame is correct).

5 TERTIARY PALAEORECONSTRUCTIONS AND THE ICELAND HOTSPOT

The combined North America–Eurasia APW path discussed above (Table 1) included 15 palaeomagnetic poles from the NAIP (UK, Ireland and the Faeroes); the addition of 10 NAIP poles from Greenland, adjusted for Labrador seafloor spreading (Roest & Srivastava 1989), does not change Palaeocene mean poles significantly. North America-Europe mean poles have been recalculated with an 8 per cent octupole non-dipole field contribution (Table 1) and, within the data resolution available, the palaeomagnetic and hotspot reference schemes for the Late Cretaceous–Tertiary are reasonable matches to one another. Both data sets will therefore produce similar palaeogeographic reconstructions.

In Table 2 we have listed hotspot reconstructions for North Greenland and Europe from 95 Ma to present times. North America is interpolated from Müller *et al.* (1993), whereas the 'absolute' positions of Greenland and Eurasia (relative to this frame) are calculated from relative fits detailed in Torsvik *et al.* (2001). As an example (Fig. 4), we show a Palaeocene, *c.* 55 Ma (c. A25 time), reconstruction for the North Atlantic, immediately prior to or during the initiation of seafloor spreading in the NE Atlantic. The 'future' A24, the oldest magnetic anomaly in the NE Atlantic, shows where Greenland separated from Eurasia at around 53 Ma. We also plot the location of NAIP rocks that have a mean age within 55 ± 1 Ma (Appendix); it is interesting to note that volcanic tuffs (54.3 ± 0.5 Ma) from the Vøring margin (presently part of the Eurasian plate; Figs 1 and 2) are both spatially and time-compatible with the Traill Ø magmatism in East Greenland (54.5 ± 0.7 Ma).

Table 2. Hotspot frame Euler poles. North America interpolated from Müller *et al.* (1993). Greenland and Eurasia based on North America concatenated with relative fits outlined in Torsvik *et al.* (2001). Angle = rotation angle.

Age Ma	North America			Greenland			Eurasia		
	Lat.	Long.	Angle	Lat.	Long.	Angle	Lat.	Long.	Angle
5	46.7	73.6	0.7	46.7	73.6	0.7	51.2	336.3	−0.6
10	43.6	120.7	1.4	43.6	120.7	1.4	79.7	314.9	−1.3
15	39.3	116.1	2.4	40.2	117.0	2.2	76.8	250.0	−2.1
20	35.0	112.2	3.4	35.9	113.0	3.2	70.6	262.3	−3.1
25	37.4	111.4	4.2	37.4	111.4	4.2	65.2	265.5	−3.4
30	41.0	110.2	5.4	40.4	110.4	5.2	61.3	265.4	−3.6
35	44.0	109.1	6.5	41.8	113.0	6.3	57.9	261.7	−3.7
40	46.2	109.7	7.6	37.9	116.7	7.6	51.8	259.2	−3.8
45	47.4	111.1	9.4	33.8	113.2	9.0	40.6	262.7	−3.9
50	46.8	112.7	11.3	31.2	106.5	10.8	33.8	262.1	−4.6
55	46.5	114.3	12.9	35.9	101.5	13.0	24.5	252.0	−4.9
60	46.2	116.1	14.9	35.3	101.5	14.6	12.9	253.5	−5.2
65	46.1	118.0	17.0	31.5	104.2	15.9	4.8	259.8	−5.9
70	46.7	119.5	19.2	28.7	107.8	17.0	1.2	86.2	6.6
75	50.3	119.0	22.0	30.2	108.4	18.8	9.7	92.9	7.8
80	53.4	117.0	24.6	31.4	108.5	20.4	17.2	95.4	9.2
85	55.0	110.1	26.2	30.6	104.8	21.4	14.9	89.8	10.7
90	57.4	104.4	28.2	33.2	101.0	22.8	21.6	82.5	12.3
95	60.4	97.5	30.0	36.9	96.0	23.9	27.3	73.6	13.8
100	62.9	89.4	31.7	40.6	90.1	25.2	31.0	64.7	15.6
105	64.6	83.6	34.5	44.1	86.3	27.4	35.3	60.3	18.1
110	66.1	77.0	37.3	47.2	81.9	29.6	38.0	56.5	20.5
115	66.5	70.0	39.6	48.6	77.1	31.6	38.3	53.1	22.8
120	66.4	63.1	42.0	49.7	72.3	33.8	38.9	49.7	25.3
125	66.2	60.0	43.7	50.2	70.4	35.3	39.7	48.4	27.2
130	65.9	56.9	45.4	50.5	68.4	36.9	40.3	47.1	29.0

The Palaeocene reconstruction places most of North America and Eurasia north of 30°N in the Early Tertiary (Fig. 4), with 'Greenwich' passing through western Norway rather than the UK (longitude is fixed in the hotspot reference frame). With a relatively stationary Iceland plume located beneath West-Central Greenland, the Faeroes and northern UK igneous provinces are 1000–1250 km from the plume centre, with the Ireland igneous province even further away.

Recent evidence from tomographic investigation on the Iceland plume (Bijwaard & Spakman 1999) shows that it extends down to the core–mantle boundary with a plume diameter of less than 500 km below the mantle transition zone (*c.* 660 km), and a diameter of up to 1200 km above this boundary (Fig. 5c). This broad upper part of the plume may be due to the superposition of the Mid-Atlantic ridge system and the Iceland hotspot. This interpretation is also in agreement with models that explain the observed topographic anomalies near Iceland with a broad and cool plume head. It also appears that the plume is a tilted feature dipping to the west, broader in a N–S direction than in E–W direction (Fig. 5c). The wavy shape of the plume structure and its deflection towards the west is ascribed by Bijwaard & Spakman (1999) to flow in the mantle, and may indicate that the hotspot is not completely stable. However, a 200–250 km difference between a strictly vertical conduit position and the present position of the plume head, tilted slightly toward the west, is within the uncertainty of the hotspot reference frame and thus, within the resolution of our data set, the plume appears to be a stable feature. We speculate that the mantle flow may find its cause in the instability created by the subducting slab of the Pacific under North America. Alternatively, or additionally, the wavy shape may also result from flow generated during the opening of the North Atlantic when the plume head moved from a position beneath Greenland to the mid-oceanic ridge (Fig. 5a,b).

The Iceland plume-head has lateral branches (between 250 km to a depth of 1000 km), the most important of which extend under Greenland as far as the Labrador Sea, with smaller ones extending under Norway and the UK (Fig. 5c). While located under Greenland (Fig. 5a), the Icelandic plume may have caused lateral flow of mantle material towards the subsequent Mid-Atlantic Ridge. Once under the Mid-Atlantic Ridge (Fig. 5b), flow would most likely have occurred along the ridge axes (Yale & Morgan 1998).

Numerical modelling of mantle plumes has, in some instances, produced slightly different hotspot positions at specific time intervals, compared to those positions generated from plate reconstructions. Notably for the Iceland plume, a recent study by Steinberger (2000), based on three different mantle models, estimated that the Iceland plume has moved toward the WSW (230–235°; his Table 2) for the last 60 million years. Hotspot motion in his analysis is calculated to be 0.6 cm yr^{-1}, considerably slower than the absolute velocities for North America–Greenland–Eurasia. If correct, this velocity would have placed the Iceland plume *c.* 333 km toward the ENE relative to our model at 55 Ma (see Fig. 4). Regardless which of these two positions is preferred for the plume at this time, the Iceland plume remains positioned beneath central Greenland

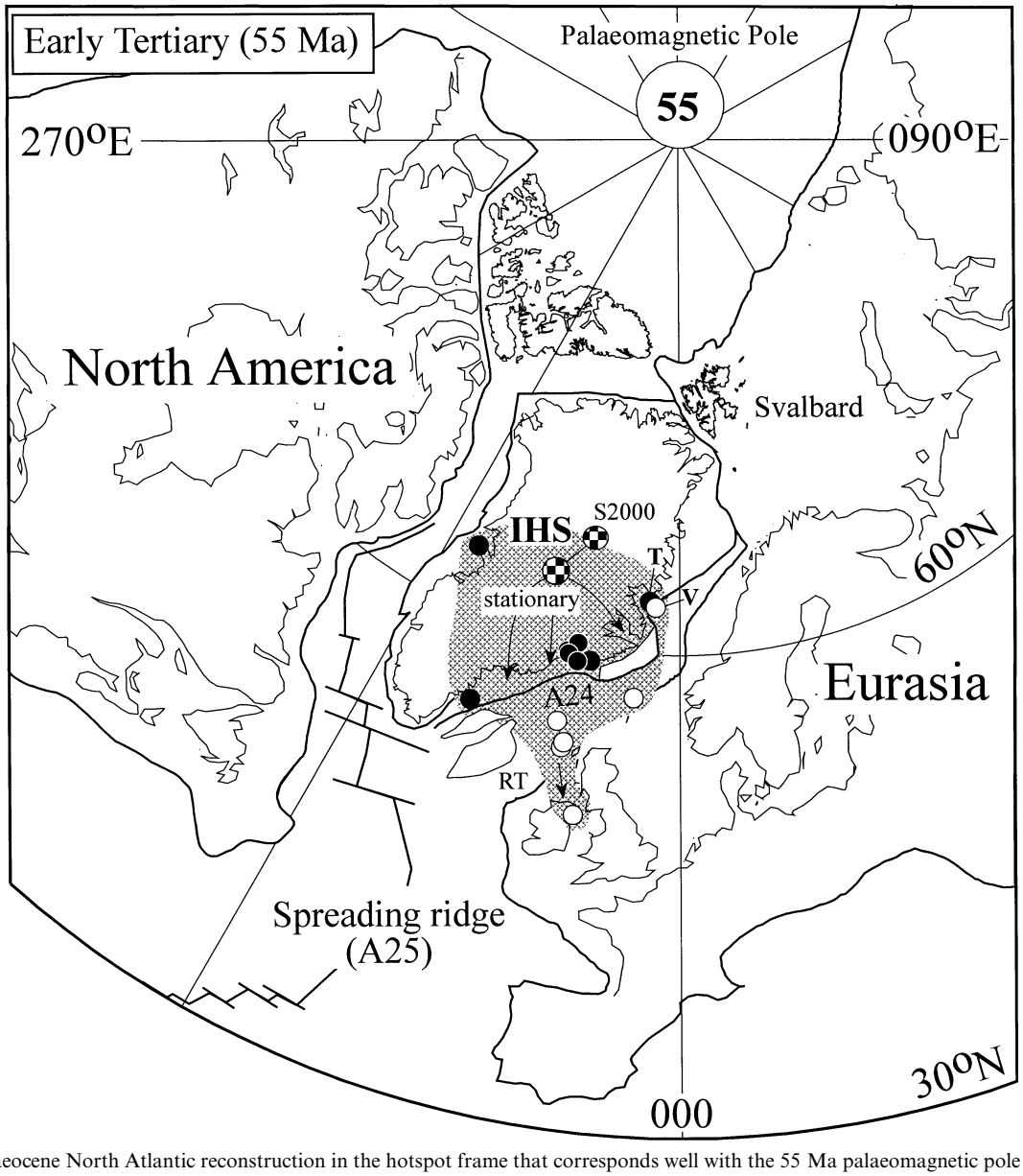

Figure 4. Palaeocene North Atlantic reconstruction in the hotspot frame that corresponds well with the 55 Ma palaeomagnetic pole with respect to this reference (shown as A95 circle). Approximate position of spreading ridge in the central Atlantic and the Labrador Sea estimated from A25 data (Müller *et al.* 1997). Approximate position of the first known magnetic anomaly (A24) in the NE Atlantic from digital data set of Skogseid *et al.* (2000) The Iceland hotspot is positioned under Greenland (IHS) and shown in two different locations: stationary or adjusted (S2000) for 0.6 cm/ year. WSW movements (230–235°) of the plume (Steinberger 2000). The latter amounts to 333 km for the last 55 Ma. The reconstructed locations for NAIP rocks with mean ages between 54 and 56 Ma (Appendix) are shown as solid (now part of the North America-Greenland plate) and open (now part of the Eurasian plate) circles. V = Vøring; T = Traill Ø.

at the initial break up in the NE Atlantic and thus, is in an appropriate location in either case to generate the observed spread of igneous products around the NAIP.

6 PLATE DIRECTIONS AND GLOBAL STRESS

Based on the 'absolute' rotation parameters for North America, Greenland and Eurasia (Table 2) we calculated the palaeo-position for a selected geographical location (for each continent) at progressive time intervals (Fig. 6), and the directional trends reveal some important and interesting features for the past 95 Ma (Early Cretaceous excluded due to potential TPW). All continents show pronounced NNE directional movements during the Late Cretaceous, followed by an abrupt NW shift at *c.* 80 Ma which is time-compatible with the oldest proposed magnetic anomaly in the Labrador Sea (A33; Roest & Srivastava 1989). A clear exception to the systematic 80 Ma NW drift pattern is the Eurasian plate that, for the last 20 million years (Fig. 6), shows a gradual change to a NE course. A small NE excursion for Eurasia (55–45 Ma) is also noted during the initial break up of the NE Atlantic. The timing of this excursion corresponds to the apparent cessation of magmatic activity in the NW Scotland–Ireland region (see previous geochronological analysis) and may reflect 'capture' of the Iceland plume on the eastern Greenland margin as seafloor

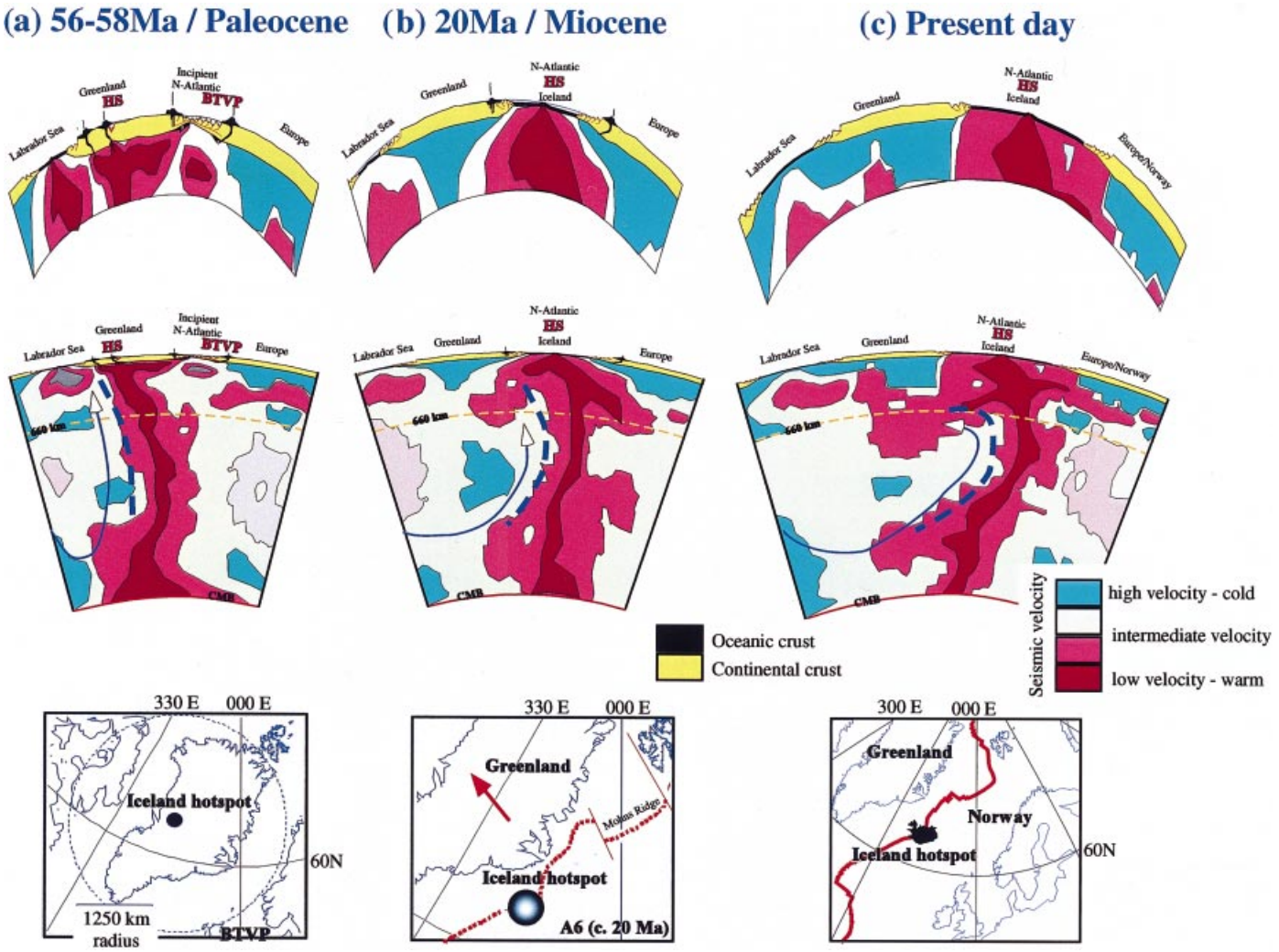

Figure 5. Present-day tomographic image (c) of the Iceland hotspot plume (modified from Bijwaard & Spakman 1999) and possible palaeo-tomography cartoon of the Iceland hotspot in its Miocene and Palaeocene position according to the hotspot frame (a-b). The position and geometry of the plume is 'reconstructed' to highlight the proportions and extent of the possible interference of an existing plume with the opening Labrador Sea and Norwegian-Greenland Sea, and their corresponding mid-ocean ridge magmatic chambers. Present-day tomography suggests a rather narrow chimney reaching from the core–mantle boundary to the surface. The hotspot reaches the North Atlantic mid-ocean ridge around 20 Ma. The large shallow-depth diverticulations observed in the present-day situation may possibly result from former connections with the mid-ocean ridge magmatic reservoirs of the Labrador Sea and the Greenland-Norwegian Sea, as well as the spreading of the plume head under the screening shield of Greenland. From the palaeo-tomographic cartoon it appears that the intrusions and the volcanism observed in Greenland and especially on the European margin of the North Atlantic (British Isles: British Tertiary volcanism province, Vøring Basin) may result from the combined input of the hotspot and the mid-ocean ridge systems developing. The age and position of the plume head is thus not in a simple relation to the different magmatic provinces investigated in recent literature (see text for discussion). The present-day inclined position of the hotspot may suggest lateral changes in mantle scale convection cells. These lateral changes may be related to the important eastward-dipping subduction of the Pacific ocean under the North American craton (the subduction reaches the core–mantle boundary under the eastern passive margin of the Central-North Atlantic). The core–mantle interface of the hotspot remains stationary while the lithospheric tectonic plates move over its head. Bottom diagrams show the geographical location of the Iceland hotspot with respect to the hotspot frame.

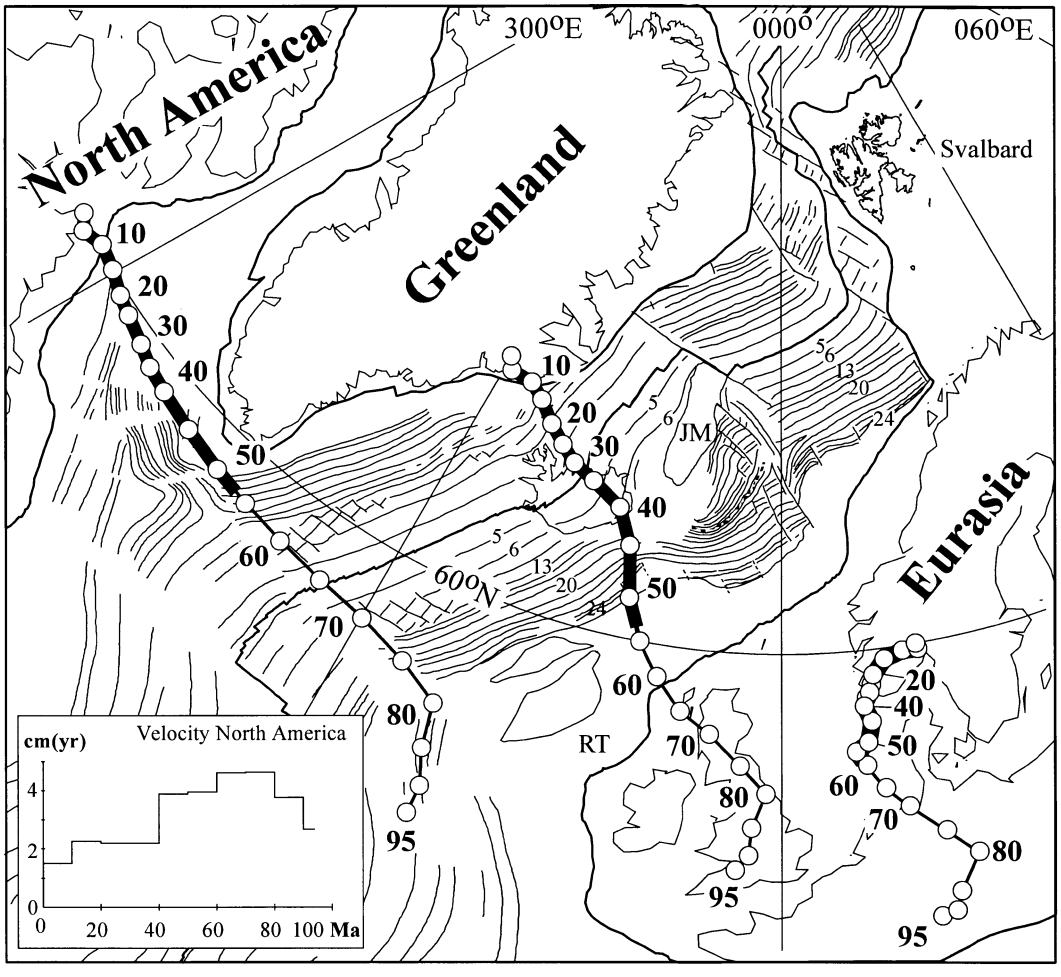

Figure 6. Track of selected locations from North America (60°N, 295°E), Greenland (69°N, 330°E) and Eurasia (60°N, 10°E) for the last 95 Myr according to the hotspot frame. Major changes in direction of all plates occur at 80 Ma from a NNE directed motion towards a NW directed displacement. At *c*. 20 Ma an important change occurs in the motion direction of Europe from NW to NE (see also present-day plate-motion in Fig. 7). Magnetic anomaly data in digital form from Skogseid *et al*. (2000; NE Atlantic) and Müller *et al*. (1997). Inset diagram shows the 'absolute' velocity for North America.

spreading commenced at 53–56 Ma. The NE course for Eurasia for the last 20 million years shows the same trend as current plate movement direction of Europe (Fig. 7) based on global positioning satellite (GPS) and satellite laser ranging (SLR) measurements. Similarly GPS and SLR data for North America–Greenland are in broad agreement with the NW to NNW directional paths derived from our analysis (Fig. 7).

All three plates show maximum velocities in the Late Cretaceous–Early Tertiary (peak of 4.6 cm yr^{-1} for North America) followed by a general decrease during most of the Tertiary (Fig. 6 inset diagram). Average velocities for Europe (1.1 cm yr^{-1}) and North America–Greenland (1.9 cm yr^{-1}) since the Early Miocene (*c*. 20 Ma) are in reasonably good agreement with, though slightly slower than, average velocities of 2–3 cm yr^{-1} obtained from present-day GPS and SLR measurements (Bianco *et al*. 1998) (Fig. 7).

When comparing worldwide stress data with plate motion, it can be seen that the plate movement directions are quite different from the stress orientations, especially in domains of passive margins and plate interiors (Zoback 1992). Stresses within the lithospheric plates reflect extension and compression due to body forces and surface tractions linked to thermally induced gravitational instabilities, and while forces at subduction zones balance, it appears that plate-wide stress field is generated by the gravitational forces at mid-ocean ridges (Engelder 1993). Ridge-push arises from the elevation of the mid-oceanic ridge and the difference in depth of the margins. The increasing depth to the ocean floor, when moving away from the ridge, is explained by the progressive cooling and accretion of lithosphere that becomes progressively denser, away from the spreading centre. The gravitational stress field thus generated on the lithosphere is compressional and roughly normal to the ridge axis. It has been shown that ridge-push affects the stable interior of plates only after some 35 Myr of cooling.

At present, broadly NW to NNW compression over large portions of the European continent suggest that intraplate stress in the North Atlantic region is related to ridge push (Wdowinski 1998; Gölke & Brudy 1996; Gölke & Coblentz 1996; Richardson 1992; Wuming *et al*. 1992). However, given the discrepancy in absolute plate motion and the global stress field in the North Atlantic region, ridge push can be excluded as a main driving mechanism for the plate drift. If purely ridge-push dominated, we would expect to see North America and

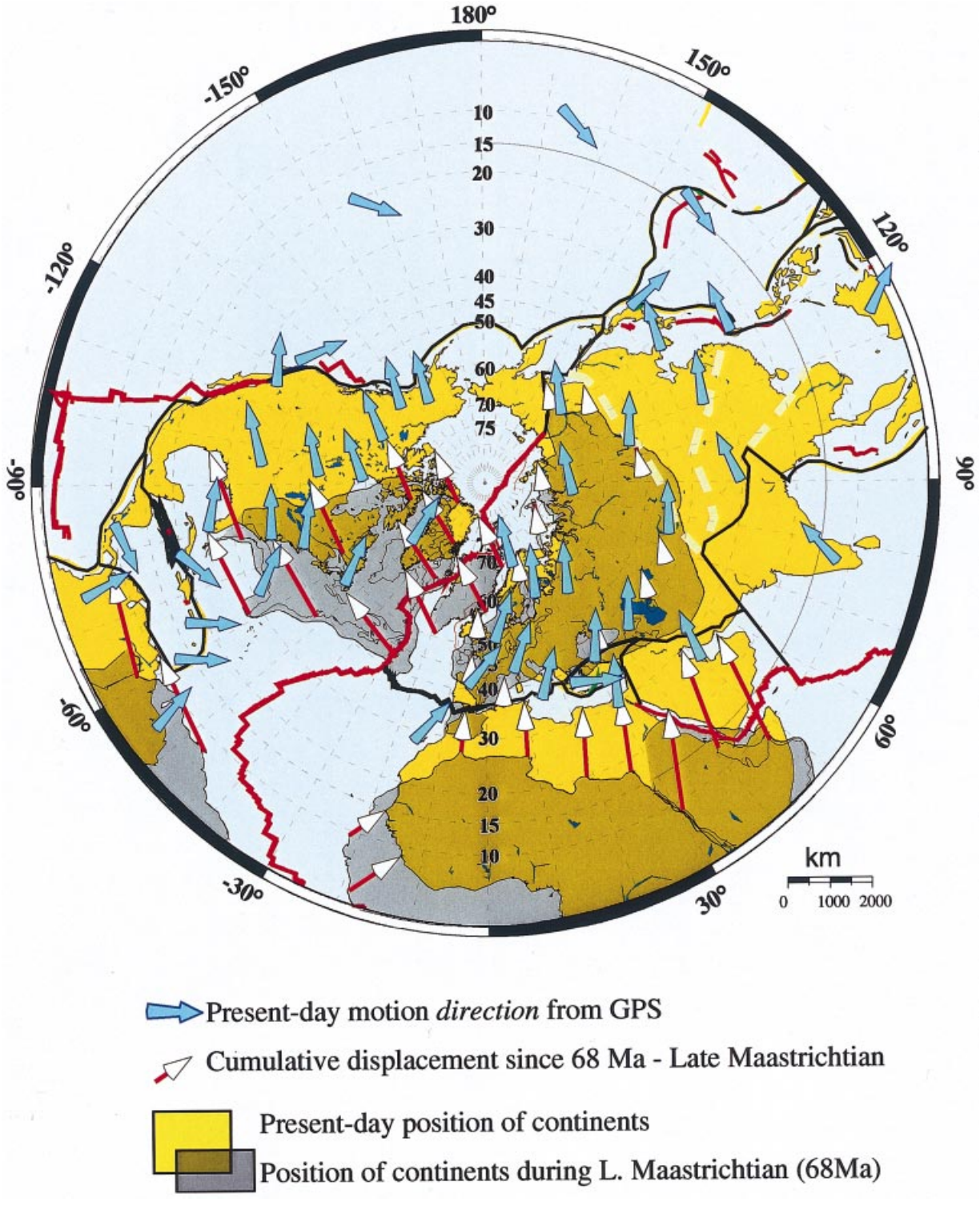

Figure 7. Present-day directions of absolute displacements of plates (large arrows from GSP/SLR measurements) and averaged plate displacement between Late Cretaceous (68 Ma) and present day position from plate reconstruction in the hotspot reference frame. Overall directions of motion for the last 68 Ma are the same as present-day motion for Eurasia and North America, with the exception of E and NE continental North America (motion direction NNE rather than E) east of the New Madrid rift zone. The data (143 sites) were obtained from the global GPS receiver network (ITRF96; International GPS Service for Geodynamics-IGS/Jet Propulsion Laboratory: http://sideshow.jpl.nasa.gov/mbh/series.htm). SLR data from Bianco *et al.* (1998).

Greenland diverging from one another at *c.* 80 Ma (opening of the Labrador Sea), and subsequently, to see Greenland diverging from Eurasia from *c.* 55 Ma (opening of the NE Atlantic). The North America–Greenland–Europe directional pathways do not show this to be the case, and we can regard ridge-push as 'unimportant' in the overall North Atlantic plate motion scenario, while it does remain a factor when considering intraplate stresses.

7 CONCLUSIONS

Given the similarity between the Late Cretaceous and Early Tertiary hotspot and palaeomagnetic reconstructions, we argue that hotspot reconstructions represent viable first-order approximations to use in plate tectonic modelling for the past 95 Ma. Minor discrepancies can be explained by a long-term, octupole non-dipole field (8 per cent) in the palaeomagnetic record. Prior to 95 Ma, the palaeomagnetic and hotspot reference differs substantially (*c.* 20°); this difference is best explained by a TPW event due to mass redistribution in the mantle. This event is contemporaneous with the Cretaceous Normal Superchron.

In the hotspot frame our analysis suggest a strong NW directional mode for North America–Greenland–Eurasia since the Late Cretaceous. The plates move fairly synchronously throughout this time period (with noted exception of Eurasia for the last 20 million years and a minor NE excursion between 55 and 45 Ma) and the overall tectonic evolution in the North Atlantic thus appears to have been dominated by external and more 'global' dynamics rather than by ridge push alone. If plates with near N-S ridge-axis geometries were purely controlled by ridge push, they should produce E-W pathways. However, we observe a communal NW movement during most of the Late Cretaceous and Tertiary, and hence must introduce a strong NW external force component in order to understand the observed pathways. These necessary external forces could comprise any combination of plate tectonic forces (external slab pull), or plate motions dominated by deeper-seated mantle factors, such as unidirectional horizontal flow (Pavoni 1993) in the upper mantle.

Mantle and crust processes are linked via complex and enigmatic cause-and-effect relationships, but the NW directional change in North Atlantic paths broadly corresponds to the oldest known magnetic anomaly from the Labrador Sea (A33), and on a global scale, coincides with separation of Greater India and Seychelles from Madagascar and a corresponding NW directional change, although less pronounced, for the African plate. These activities were coeval with the peri-Arabic ophiolite obduction, deformation in the Syrian arc and intra-oceanic subduction in front of the northward migrating Indian continent, thus indicating an active global framework for contemporary North Atlantic motions.

The NE directional trend for Eurasia for the last 20 Myr is compatible with present day GPS and SLR measurements. The NE shift in plate motion is similar to that of Africa and may suggest a stronger 'plate-coupling' between Africa and Eurasia from this time; alternatively, this directional shift could be linked with positioning of the Iceland plume below the spreading axis at *c.* 20 Ma. Irrespective of its external origin, the 'unified' NW movement of North America-Greenland-Eurasia during most of the Tertiary (velocities of up to 4.6 cm/ year.) was the deciding factor in establishing the position of the Icelandic plume at the eastern trailing edge of the NE Atlantic well into the Tertiary, and hence long after initial opening. Subduction (slab pull) is generally considered to be the most important force in running the plate tectonic machinery (Forsyth & Uyeda 1975; Lithgow-Bertelloni & Richards 1998), but the relation between shallow (slab pull and ridge push) and deep mantle driving forces is not obvious. Shallow upwelling does occur below spreading ridges, but is probably unrelated to large-scale mantle flow patterns since spreading ridges are non-stationary. In the NE Atlantic, the spreading ridge migrated north-westward (external force control) with the result that the Iceland plume has been close to the spreading ridge for the last 20 million years. This positioning of the plume beneath the ridge may certainly have increased upwelling below the spreading ridge, increased the ridge-push, and caused a NE shift in the absolute direction of Eurasia.

ACKNOWLEDGMENTS

This research was funded by VISTA (Norwegian Academy of Sciences and Statoil), the Geological Survey of Norway, the BAT project (BP Amoco, Mobil Exploration Norway Inc., Norsk Hydro ASA, Norsk Agip A/S, Norske Conoco AS, Norske Chevron A/S, Norske Shell, Phillips Petroleum Company Norway, Saga Petroleum and Statoil) and the Norwegian Research Council. Two anonymous reviewers are thanked for useful comments.

REFERENCES

Besse, J. & Courtillot, V., 1991. Revised and synthetic apparent polar wander paths for the African, Eurasian, North American and Indian plates, and true polar wander since 200 Ma, *J. geophys. Res.,* **96,** 4029–4050.

Bianco, G., Devoti, R., Fermi, M., Luceri, V., Rutigliano, P. & Sciarretta, C., 1998. A contribution in the estimation of tectonic motion in crucial areas: the CGS96 SLR solution, *Tectonophysics,* **294** 225–236.

Bijwaard, H. & Spakman, W., 1999. Tomographic evidence for narrow whole mantle plume below Iceland, *Earth planet. Sci. Lett.,* **166,** 121–126.

Brooks, C.K. & Gleadow, A.J.W., 1977. A fission-track age for the Skaergaard intrusion and the age of the East Greenland basalts, *Geology,* **5,** 539–540.

Bugge, T., Prestvik, T. & Rokoengen, K., 1980. Lower Tertiary volcanic rocks off Kristiansund-Mid Norway, *Mar. Geol.,* **35,** 215–220.

Cande, S.C. & Kent, D.V., 1995. Revised calibration of the geomagnetic polarity timescale for the Late Cretaceous and Cenozoic, *J. geophys. Res.,* **100,** 6093–6095.

Courtillot, V. & Besse, J., 1987. Magnetic field reversals, polar wander, and core-mantle coupling, *Science,* **237,** 1140–1147.

Courtillot, V., Jaupart, C., Manighetti, I., Taponnier, P. & Besse, J., 1999. On causal links between flood basalts and continental breakup, *Earth planet. Sci. Lett.,* **166,** 177–195.

Dickin, A.P., 1981. Isotope geochemistry of Tertiary igneous rocks from the Isle of Skye, NW Scotland, *J. Petrol.,* **22,** 155–189.

Dickin, A.P. & Jones, N.W., 1983. Isotopic evidence for the age and origin of pitchstones and felsites, Isle of Eigg, NW Scotland, *J. geol. Soc. Lond.,* **140,** 691–700.

Eide, E.A. & Torsvik, T.H., 1996. Paleozoic supercontinental assembly, mantle flushing, and genesis of the Kiaman Superchron, *Earth planet. Sci. Lett.,* **144,** 389–402.

Engelder, T., 1993. *Stress Regimes in the Lithosphere,* Princeton University Press, Princeton.

Forsyth, D. & Uyeda, S., 1975. On the relative importance of the driving forces of plate motion, *Geoph. J. R. astr. Soc.,* **43,** 163–200.

Gallet, Y. & Hulot, G., 1997. Stationary and nonstationary behaviour within the geomagnetic polarity time scale, *Geophys. Res. Lett.,* **24,** 1875–1878.

Gamble, J.A., Wysoczanski, R.J. & Meighan, I.G., 1999. Constraints on the age of the British Tertiary Volcanic Province from ion microprobe U-Pb (SHRIMP) ages for acid igneous rocks from NE Ireland, *J. geol. Soc. Lond.,* **156,** 291–299.

Gibson, D., McCormick, A.G., Meighan, I.G. & Halliday, A.N., 1987. The British Tertiary Igneous Province: Young Rb-Sr ages for the Mourne Mountains granites, *Scott. J. Geol.,* **23,** 221–225.

Gleadow, A.J.W. & Brooks, C.K., 1979. Fission track dating, thermal histories and tectonics of igneous intrusions in East Greenland, *Contrib. Mineral. Petrol.,* **71,** 45–60.

Gölke, M. & Brudy, M., 1996. Orientation of crustal stresses in the North Sea and Barents Sea inferred from borehole breakouts, *Tectonophysics,* **266,** 25–32.

Gölke, M. & Coblentz, D., 1996. Origins of the European regional stress field, *Tectonophysics,* **266,** 11–24.

Gordon, R.G., 1987. Polar wandering and palaeomagnetism, *Ann. Rev. Earth Planet. Sci.,* **15,** 567–593.

Gurnis, M. & Torsvik, T.H., 1994. Rapid drift of large continents during the late Precambrian and Paleozoic: Paleomagnetic constraints and dynamic models, *Geology,* **22,** 1023–1026.

Hirschmann, M.M., Renne, P.R. & McBirney, A.R., 1997. $^{40}Ar/^{39}Ar$ dating of the Skærgaard intrusion, *Earth planet. Sci. Lett.,* **146,** 645–658.

Hitchen, K. & Ritchie, J.D., 1993. New K-Ar ages, and a provisional chronology, for the offshore part of the British Tertiary Igneous Province, *Scott. J. Geol.,* **29,** 73–85.

Johnson, H.P., Van Patten, D., Tivey, M. & Sager, W.W., 1995. Geomagnetic polarity reversal rate for the Phanerozoic, *Geophys. Res. Lett.,* **22,** 231–234.

Jurdy, D.M., 1981. True polar wander, *Tectonophysics,* **74,** 1–16.

Larson, R.L. & Olson, P., 1991. Mantle plumes control magnetic reversal frequency, *Earth planet. Sci. Lett.,* **107,** 437–447.

Lawver, L.A. & Müller, R.D., 1994. Iceland hotspot track, *Geology,* **22,** 311–314.

Lithgow-Bertelloni, C. & Richards, M.A., 1998. The dynamics of Cenozoic and Mesozoic plate motions, *Rev. Geophys.,* **36,** 27–78.

Lottes, A.L. & Rowley, D.B., 1990. Reconstruction of the Laurasian and Gondwana segments of Permian Pangaea, in *Palaeozoic Palaeogeography and Biogeography*, pp. 383–395, eds McKerrow, W.S. & Scotese, C.R., *Geol. Society Lond. Mem.*, 12, Geological Society, London.

McElhinny, M., 1971. Geomagnetic reversals during the Phanerozoic, *Science,* **172,** 157–159. 1971.

McElhinny, M.W., McFadden, P.L. & Merrill, R.T., 1996. The time-averaged paleomagnetic field 0–5 Ma, *J. geophys. Res.,* **101,** 25 007–25 027.

Müller, R.D., Roest, W.R., Royer, J.-Y., Gahagan, L.M. & Sclater, J.G., 1997. Digital Isochrons of the Worlds's Ocean floor, *J. geophys. Res.,* **102,** 3211–3214.

Müller, R.D., Royer, J.Y. & Lawver, L.A., 1993. Revised plate motions relative to the hotspots from combined Atlantic and Indian Ocean hotspot tracks, *Geology,* **21,** 275–278.

Mussett, A.E., 1984. Time and duration of Tertiary igneous activity of Rhum and adjacent areas, *Scott. J. Geol.,* **20,** 273–279.

Mussett, A.E., 1986. ^{40}Ar-^{39}Ar step-heating ages of the Tertiary igneous rocks of Mull, Scotland, *J. geol. Soc. Lond.,* **143,** 887–896.

Nevle, R.J., Brandriss, M.E., Bird, D.K., McWilliams, M.O. & O'Neil, J.R., 1994. Tertiary plutons monitor climate change in East Greenland, *Geology,* **22,** 775–778.

Noble, R.H., Macintyre, R.M. & Brown, P.E., 1988. Age constraints on Atlantic evolution: Timing of magmatic activity along the E Greenland continental margin, *J, Geol. Soc. Spec. Pub., Early Tertiary Volcanism and the Opening of the NE Atlantic,* **39,** 201–214.

Norton, I.O., 1995. Plate motions in the North Pacific: the 43 Ma nonevent, *Tectonics,* **14,** 1080–1094.

Opdyke, N.D. & Channell, J.E.T., 1996. *Magnetic Stratigraphy,* Academic Press Inc, London.

Pavoni, N., 1993. Pattern of mantle convection and Pangea break-up, as revealed by the evolution of the African plate, *J. geol. Soc. Lond.,* **150,** 953–964.

Pearson, D.G., Emeleus, C.H. & Kelley, S.P., 1996. Precise $^{40}Ar/^{39}Ar$ age for the initiation of Palaeogene volcanism in the Inner Hebrides and its regional significance, *J. geol. Soc. Lond.,* **153,** 815–818.

Prévot, M., Mattern, E., Camps, P. & Daignierès, M., 2000. Evidence for a 20° tilting of the Earth's rotation axis 110 million years ago, *Earth planet. Sci. Lett.,* **179,** 517–528.

Price, S., Brodie, J., Whitham, A. & Kent, R., 1997. Mid-Tertiary rifting and magamatism in the Traill Ø region, East Greenland, *J. geol. Soc. Lond.,* **154,** 419–434.

Richardson, R.M., 1992. Ridge forces, absolute plate motion, and intraplate stress field, *J. geophys. Res.,* **97,** 11 739–11 748.

Roest, W.R. & Srivastava, S.P., 1989. Sea-floor spreading in the Labrador Sea: a new reconstruction, *Geology,* **17,** 1000–1003.

Rowley, D.B. & Pindell, J.L., 1989. End Paleozoic-Early Mesozoic western Pangean reconstruction and its implications for the distribution of Precambrian and Paleozoic rocks around Meso-America, *Precam. Res.,* **42,** 411–444.

Saunders, A.D., Fitton, J.G., Kerr, A.C., Norry, M.J. & Kent, R.W., 1997. The North Atlantic Igneous province, in *Large Igneous Provinces, Geophysical Monograph 100,* pp. 45–93, eds. Mahoney, J.J. & Coffin, M.F., *American Geophysical Union,* Washington, DC.

Sinton, C.W. & Duncan, R.A., 1998. ^{40}Ar-^{39}Ar ages of lavas from the southeast Greenland margin, ODP leg 152, and the Rockall Plateau, DSDP leg 81, *Proc. Ocean Drilling Prog.,* **152,** 387–402.

Sinton, C.W., Hitchen, K. & Duncan, R.A., 1998. ^{40}Ar-^{39}Ar geochronology of silicic and basic volcanic rocks, *Geol. Mag.,* **135,** 161–170.

Skogseid, J., Planke, S., Faleide, J.I., Pedersen, T., Eldhom, O. & Neverdal, F., 2000. NE Atlantic continental rifting and volcanic margin formation, in *Dynamics of the Norwegian Margin, Geol, Society Lond, Spec. Pub., 167,* pp. 295–326, eds Nøttvedt, *et al.*, Geological Society, London.

Srivastava, S.P. & Roest, W.R., 1989. Seafloor spreading history II-IV, in *East Coast Basin Atlas Series: Labrador Sea,* ed. Bell, J.S., Atlantic Geoscience Centre, Geologic Survey of Canada, Ottawa, Map sheets L17–2 – L17–6.

Steinberger, B., 2000. Plumes in a convecting mantle: Models and observation for individual hotspots, *J. geophys. Res.,* **105,** 11127–11152.

Steinberger, B. & O'Connell, R.J., 1998. Advection of plumes in mantle flow: implications for hotspot motion, mantle viscosity and plume distribution, *Geophys. J. Int.,* **132,** 412–434.

Storey, M., Duncan, R.A., Pedersen, A.K., Larsen, L.M. & Larsen, H.C., 1998. $^{40}Ar/^{39}Ar$ geochronology of the West Greenland Tertiary volcanic province, *Earth planet. Sci. Lett.,* **160,** 569–586.

Tarduno, J.A. & Cottrell, R.D., 1997. Paleomagnetic evidence for motion of the Hawaiian hotspot during formation of the Emperor seamounts, *Earth planet. Sci. Lett.,* **153,** 171–180.

Tegner, C. & Duncan, R.A., 1999. ^{40}Ar-^{39}Ar chronology for the volcanic history of the southeast Greenland rifted margin LEG163, *Proc. Ocean Drilling Prog., Sci. Res.,* **163,** 53–62.

Tegner, C., Duncan, R.A., Bernstein, S., Brooks, C.K., Bird, D.K. & Storey, M., 1998. ^{40}Ar-^{39}Ar geochronology of Tertiary mafic intrusions along the East greenland rifted margin: Relation to flood basalts and the Iceland hotspot track, *Earth planet. Sci. Lett.,* **156,** 75–88.

Thompson, P., Mussett, A.E. & Dagley, P., 1987. Revised ^{40}Ar-^{39}Ar age for granites of the Mourne Mountains, Ireland, *Scott. J. Geol.,* **23,** 215–220.

Torsvik, T.H. & Eide, E.A., 1998. NGU GEOCHRON: Database and analysis package for Norwegian isotope geochronology, *NGU Report 98.002.*

Torsvik, T.H., Smethurst, M.A., Meert, J.G., Van der Voo, R., McKerrow, W.S., Brasier, M.D., Sturt, B.A. & Walderhaug, H.J., 1996. Continental break-up and collision in the Neoproterozoic and Paleozoic—A tale of Baltica and Laurentia, *Earth-Sci. Rev.,* **40,** 229–258.

Torsvik, T.H., Van der Voo, R., Meert, J.G., Mosar, J. & Walderhaug, H.J., 2001. Late Palaeozoic-Early Tertiary palaeomagnetic data from North America and Eurasia: Revised APW paths and reconstruction fits, *Earth planet. Sci. Lett.,* **187,** 55–69.

Upton, B.G.J., Emeleus, C.H., Rex, D.C. & Thirlwall, M.F., 1995. Early Tertiary magamatism in NE Greenland, *J. geol. Soc. Lond.,* **152,** 959–964.

Van der Voo, R. & Torsvik, T.H., 2001. Evidence for Permian and Mesozoic non-dipole fields provides and explanation for the Pangea reconstruction problems, *Earth planet. Sci. Lett.,* **187,** 71–81.

Van Fossen, M.C. & Kent, D., 1992. Paleomagnetism of 122 Ma plutons in New England and the Mid-Cretaceous Paleomagnetic field in North America: True polar wander or large-scale differential mantle motion? *J. geophys. Res.,* **97,** 19 651–19 661.

Wdowinski, S., 1998. A theory of intraplate tectonics, *J. geophys. Res.,* **103,** 5037–5059.

Weinstein, S.A., 1993. Catastrophic overturn of the Earth's mantle driven by multiple phase changes and internal heat generation, *Geophys. Res. Lett.,* **20,** 101–104.

Wuming, B., Vigny, C., Ricard, Y. & Froidevaux, C., 1992. On the origin of deviatoric stress in the lithosphere, *J. geophys. Res.,* **97,** 11 729–11 737.

Yale, M.M. & Morgan, J.P., 1998. Asthenosphere flow model of hotspot—ridge interactions: a comparison of Iceland and Kerguelen, *Earth planet. Sci. Lett.,* **161,** 45–56.

Zoback, M.L., 1992. First- and second-order patterns of stress in the lithosphere: the World Stress Map project, *J. geophys. Res.,* **97,** 11 703–11 728.

APPENDIX A: COMPILATION OF THE MOST RELIABLE GEOCHRONOLOGICAL DATA FROM THE NORTH ATLANTIC IGNEOUS PROVINCE

Age	$\pm 2\sigma$	Method	Mineral	Rock Type	Lat.	Long.	Author
21.4	1	K–Ar	Whole rock	Dyke	72.1	−23.6	Noble *et al.* (1988)
21.5	1	K–Ar	Whole rock	Dyke	72.1	−23.6	Noble *et al.* (1988)
27.4	0.6	Ar–Ar	Whole rock	Alkali basalt	70.09	−54.9	Storey *et al.* (1998)
28.1	1.4	K–Ar	Amphibole	Dyke	72.1	−23.6	Noble *et al.* (1988)
28.9	1	K–Ar	Biotite	Dyke	72.1	−23.6	Noble *et al.* (1988)
29.3	1.2	K–Ar	Biotite	Granite	67	−33.5	Noble *et al.* (1988)
30.1	1.4	K–Ar	Amphibole	Dyke	72.1	−23.6	Noble *et al.* (1988)
30.3	2	K–Ar	Biotite	Dyke	72.1	−23.6	Noble *et al.* (1988)
30.3	2.6	FT	Titanite	Quartz syenite	72	−24.8	Gleadow & Brooks (1979)
32.6	1.2	K–Ar	Biotite	Lamprophyre dyke	67	−33.5	Noble *et al.* (1988)
32.7	1.2	Ar–Ar	Whole rock	Picritic dolerite	73.2	−21	Upton *et al.* (1995)
33.9	1.4	K–Ar	Amphibole	Granite	72.8	−22.5	Noble *et al.* (1988)
34	1.4	K–Ar	Whole rock	Lamprophyre dyke	67	−33.5	Noble *et al.* (1988)
34.1	0.2	Ar–Ar	K-Feldspar	Lamprophyre dyke	71.21	−53.9	Storey *et al.* (1998)
34.1	4.4	K–Ar	Pyroxene	Granite	72.8	−22.5	Noble *et al.* (1988)
34.2	1.6	K–Ar	Amphibole	Lamprophyre dyke	67	−33.5	Noble *et al.* (1988)
34.2	4	K–Ar	Amphibole	Lamprophyre dyke	68.4	−28	Noble *et al.* (1988)
34.8	3.4	K–Ar	Amphibole	Lamprophyre dyke	68.4	−28	Noble *et al.* (1988)
35.4	1.6	K–Ar	Amphibole	Granite	72.8	−22.5	Noble *et al.* (1988)
35.4	1.8	K–Ar	Amphibole	Lamprophyre dyke	67	−33.5	Noble *et al.* (1988)
35.8	1.2	K–Ar	Amphibole	Lamprophyre dyke	68.4	−28	Noble *et al.* (1988)
36.2	0.6	Ar–Ar	Whole rock	Alkali basalt dyke	72.7	−22	Price *et al.* (1997)
36.2	0.8	FT	Mixed	Granite complex	66.8	−33.9	Gleadow & Brooks (1979)
36.5	4.2	K–Ar	Amphibole	Syenite	68	−32	Noble *et al.* (1988)
36.6	1.8	K–Ar	Whole rock	Lamprophyre dyke	67	−33.5	Noble *et al.* (1988)
36.6	2	K–Ar	Amphibole	Syenite	68	−32	Noble *et al.* (1988)
36.9	5.2	K–Ar	Pyroxene	Granite	72.8	−22.5	Noble *et al.* (1988)
36.9	0.4	Ar–Ar	Whole rock	Alkaline basalt dyke	72.7	−22	Price *et al.* (1997)
37.1	1.6	K–Ar	Amphibole	Syenite	68	−32	Noble *et al.* (1988)
37.1	4	FT	Apatite	Gabbro	67.78	−32.3	Gleadow & Brooks (1979)
39	1.8	K–Ar	Amphibole	Syenite	68	−32	Noble *et al.* (1988)
39.3	2.2	FT	Titanite(Sphene)	Late dyke	68.25	−32.5	Gleadow & Brooks (1979)
40.4	3.6	K–Ar	Amphibole	Syenite	68	−32	Noble *et al.* (1988)
40.7	1.6	K–Ar	Amphibole	Syenite	68	−32	Noble *et al.* (1988)
40.8	1.8	K–Ar	Amphibole	Syenite	68	−32	Noble *et al.* (1988)
40.9	2.2	K–Ar	Whole rock	Alkaline basalt	69	−31	Noble *et al.* (1988)
41.2	1.4	K–Ar	Biotite	Syenite	68	−32	Noble *et al.* (1988)
41.2	1.4	K–Ar	Biotite	Syenite	68	−32	Noble *et al.* (1988)
41.6	2.4	K–Ar	Amphibole	Syenite	68	−32	Noble *et al.* (1988)
41.6	1.4	K–Ar	Biotite	Syenite	68	−32	Noble *et al.* (1988)
41.9	3.2	K–Ar	Whole rock	Alkaline basalt	69	−31	Noble *et al.* (1988)
42.1	1	Ar–Ar	Amphibole	Hydrothermal vein	68.16	−32	Nevle *et al.* (1994)
42.1	1.6	K–Ar	Biotite	Syenite	68	−32	Noble *et al.* (1988)
42.6	1.8	K–Ar	Amphibole	Dark syenite	68.8	−28	Noble *et al.* (1988)
42.9	1.4	K–Ar	Biotite	Syenite	68	−32	Noble *et al.* (1988)
43	2.8	FT	Titanite	Late dyke	68.25	−32.5	Gleadow & Brooks (1979)
43.1	4.6	K–Ar	Biotite	Syenite	68	−32	Noble *et al.* (1988)
43.2	1.4	K–Ar	Biotite	Syenite vein	68	−32	Noble *et al.* (1988)
43.8	1.6	K–Ar	Amphibole	Dark syenite	68.8	−28	Noble *et al.* (1988)
43.9	2.2	K–Ar	Amphibole	Dark syenite	68.8	−28	Noble *et al.* (1988)

Age	$\pm 2\sigma$	Method	Mineral	Rock Type	Lat.	Long.	Author
43.9	1.4	K–Ar	Biotite	Syenite vein	68	−32	Noble *et al.* (1988)
44	1.6	K–Ar	Amphibole	Dark syenite	68.8	−28	Noble *et al.* (1988)
44.1	2	FT	Zircon	Late dyke	66.2	−35	Gleadow & Brooks (1979)
44.2	1.8	K–Ar	Whole rock	Dolerite dyke	68.2	−28.5	Noble *et al.* (1988)
44.2	1.4	K–Ar	Biotite	Syenite vein	68	−32	Noble *et al.* (1988)
44.3	2.2	K–Ar	Whole rock	Dolerite dyke	68.2	−28.5	Noble *et al.* (1988)
44.3	1.8	Ar–Ar	Amphibole	Syenite	68.16	−32	Nevle *et al.* (1994)
44.6	1.6	K–Ar	Biotite	Syenite vein	67.8	−33	Noble *et al.* (1988)
45.5	1.6	K–Ar	Amphibole	Dark syenite	68.8	−28	Noble *et al.* (1988)
46.2	2.6	K–Ar	Amphibole	Metabasalt	68.3	−28.3	Noble *et al.* (1988)
46.4	1.6	K–Ar	Amphibole	Pale syenite	68.8	−28	Noble *et al.* (1988)
46.7	4.8	FT	Titanite	Nepheline syenite	68.8	−28.3	Gleadow & Brooks (1979)
47	0.4	Ar–Ar	Biotite	Gabbroic pegmatite	67.35	−32.5	Tegner *et al.* (1998)
47	1.8	K–Ar	Amphibole	Dyke	68.3	−28.3	Noble *et al.* (1988)
47	1.6	K–Ar	Biotite	Dyke	68.3	−28.3	Noble *et al.* (1988)
47	5.8	FT	Apatite	Rhyolite dyke	66.5	−34.2	Gleadow & Brooks (1979)
47.3	7.2	FT	Apatite	Gabbro	67.7	−32.5	Gleadow & Brooks (1979)
47.3	0.6	Ar–Ar	Biotite	Wehrlite sill	68.01	−32	Tegner *et al.* (1998)
47.5	2.2	K–Ar	Biotite	Metabasalt	68.3	−28.3	Noble *et al.* (1988)
47.6	1.6	K–Ar	Biotite	Metabasalt	68.3	−28.3	Noble *et al.* (1988)
48	1.8	K–Ar	Amphibole	Metabasalt	68.3	−28.3	Noble *et al.* (1988)
48	2.4	K–Ar	Plagioclase	Dolerite dyke	68.2	−28.5	Noble *et al.* (1988)
48	2.4	Ar–Ar	Biotite	Gabbroic pegmatite	67	−34.5	Tegner *et al.* (1998)
48.1	0.4	Ar–Ar	Amphibole	Gabbro	67.9	−32	Nevle *et al.* (1994)
48.1	1.8	K–Ar	Amphibole	Pale syenite	68.8	−28	Noble *et al.* (1988)
48.3	1.6	K–Ar	Amphibole	Metabasalt	68.3	−28.3	Noble *et al.* (1988)
48.4	3.2	K–Ar	Whole rock	Dolerite dyke	68.2	−28.5	Noble *et al.* (1988)
48.4	1.6	K–Ar	Biotite	Dyke	68.3	−28.3	Noble *et al.* (1988)
48.5	1.6	K–Ar	Biotite	Metabasalt	68.3	−28.3	Noble *et al.* (1988)
48.6	1.8	K–Ar	Amphibole	Pale syenite	68.8	−28	Noble *et al.* (1988)
48.6	0.4	Ar–Ar	Phlogopite	Pegmatite	68.15	−32.1	Nevle *et al.* (1994)
48.6	1.8	K–Ar	Biotite	Pegmatite	68.8	−28	Noble *et al.* (1988)
48.6	0.4	Ar–Ar	Phlogopite	Pegmatite	68.1	−32	Nevle *et al.* (1994)
48.6	1.6	K–Ar	Biotite	Metabasalt	68.3	−28.3	Noble *et al.* (1988)
48.7	3	K–Ar	Amphibole	Syenite vein	68	−32	Noble *et al.* (1988)
48.7	2.2	K–Ar	Plagioclase	Dolerite dyke	68.2	−28.5	Noble *et al.* (1988)
48.7	1	K–Ar	Whole rock	Gabbroic sill	60.5	−2.6	Hitchen & Ritchie (1993)
48.8	0.4	Ar–Ar	Amphibole	Gabbroic pegmatite	68.02	−32	Tegner *et al.* (1998)
49.2	0.4	Ar–Ar	Biotite	Wehrlite sill	66.44	−34.5	Tegner *et al.* (1998)
49.4	0.6	Ar–Ar	Plagioclase	Basalt	66	−35	Tegner & Duncan (1999)
49.4	0.6	Ar–Ar	Amphibole	Pegmatite	68.1	−32	Nevle *et al.* (1994)
49.4	3.2	K–Ar	Whole rock	Dolerite dyke	68.2	−28.5	Noble *et al.* (1988)
49.4	1	Ar–Ar	Whole rock	Basalt	66	−35	Tegner & Duncan (1999)
49.4	0.6	Ar–Ar	Amphibole	Peridotite	68.1	−32	Nevle *et al.* (1994)
49.6	1.8	K–Ar	Whole rock	Dolerite dyke	68.2	−28.5	Noble *et al.* (1988)
49.7	0.6	Ar–Ar	Whole rock	Basalt	66	−35	Tegner & Duncan (1999)
49.7	0.8	Ar–Ar	Hornblende	Pegmatite	68.1	−32	Nevle *et al.* (1994)
49.7	0.6	Ar–Ar	Amphibole	Pegmatite	68.1	−32	Nevle *et al.* (1994)
49.8	2.4	Ar–Ar	Biotite	Wehrlite sill	66.45	−34.5	Tegner *et al.* (1998)
49.9	1.6	K–Ar	Amphibole	Metabasalt	68.3	−28.3	Noble *et al.* (1988)
50	0.8	Ar–Ar	Amphibole	Syenite vein	68.31	−29	Tegner *et al.* (1998)
50	1.4	K–Ar	Whole rock	Basalt	59.2	−7.1	Hitchen & Ritchie (1993)
50.3	2.8	FT	Mixed	Alkaline ultramafic	68.66	−33.3	Gleadow & Brooks (1979)
50.4	1.8	K–Ar	Amphibole	Gabbro	68.3	−28.3	Noble *et al.* (1988)
50.5	1.8	K–Ar	Amphibole	Vein in quartz syenite	68.31	−32	Noble *et al.* (1988)
50.6	1.8	K–Ar	Biotite	Dyke	68.3	−28.3	Noble *et al.* (1988)
50.6	1.8	K–Ar	Whole rock	Lamprophyre dyke	68.2	−28.5	Noble *et al.* (1988)
50.8	1.8	K–Ar	Amphibole	Gabbro	68.3	−28.3	Noble *et al.* (1988)
50.8	5.4	FT	Zircon	Alkaline intrusive	68.31	−32.1	Brooks & Gleadow (1977)
50.8	2.8	K–Ar	Whole rock	Alkaline basalt	69	−31	Noble *et al.* (1988)
50.9	3	FT	Mixed	Kangerd intrusion	68.25	−32.5	Gleadow & Brooks (1979)
51.1	1.6	K–Ar	Whole rock	Basalt	59.2	−7.1	Hitchen & Ritchie (1993)
51.1	2	Ar–Ar	Whole rock	Basalt	66	−35	Tegner & Duncan (1999)
51.3	1.8	K–Ar	Nepheline	Vein in quartz syenite	68.31	−32.1	Noble *et al.* (1988)
51.4	2.2	K–Ar	Amphibole	Vein in quartz syenite	68.31	−32.1	Noble *et al.* (1988)

Age	$\pm 2\sigma$	Method	Mineral	Rock Type	Lat.	Long.	Author
51.6	2.4	K–Ar	Amphibole	Layered gabbro	68.3	−28.3	Noble *et al.* (1988)
51.6	9	Ar–Ar	Whole rock	Basalt	56.5	−20	Sinton & Duncan (1998)
51.9	1.2	Ar–Ar	Whole rock	Basalt sill	63.1	−38.7	Sinton & Duncan (1998)
52	2.4	K–Ar	Whole rock	Sill	68	−30	Noble *et al.* (1988)
52	2	K–Ar	Amphibole	Vein in quartz syenite	68.31	−32.1	Noble *et al.* (1988)
52.1	1	Rb–Sr	Mixed	Volcanic glass	56.8	−6.2	Dickin & Jones (1983)
52.1	1	K–Ar	Whole rock	Olivine basalt	58.9	−7	Hitchen & Ritchie (1993)
52.5	3	K–Ar	Whole rock	Sill	68	−30	Noble *et al.* (1988)
52.5	1.8	K–Ar	Amphibole	Dyke	68.3	−28.3	Noble *et al.* (1988)
52.5	5.2	FT	Titanite(Sphene)	Gabbros	67	−33.7	Gleadow & Brooks 1979
52.5	2.4	FT	Zircon	Gabbro	68.2	−29	Gleadow & Brooks (1979)
52.5	0.2	Ar–Ar	Plagioclase	Comendite tuff	70.66	−54.6	Storey *et al.* (1998)
52.7	2.6	K–Ar	Whole rock	Sill	68	−30	Noble *et al.* (1988)
52.8	1.8	K–Ar	Whole rock	Lamprophyre dyke	68.2	−28.5	Noble *et al.* (1988)
52.9	2	K–Ar	Whole rock	Dolerite	61.6	−1	Hitchen & Ritchie (1993)
53	1	K–Ar	Whole rock	Gabbroic sill	60.5	−2.6	Hitchen & Ritchie (1993)
53	5.8	K–Ar	Whole rock	Tholeiitic basalt	68	−30	Noble *et al.* (1988)
53	2	K–Ar	Whole rock	Tholeiitic basalt	68.4	−28	Noble *et al.* (1988)
53.1	2.4	K–Ar	Whole rock	Alkaline basalt	69	−31	Noble *et al.* (1988)
53.3	1	K–Ar	Whole rock	Olivine basalt	58.9	−7	Hitchen & Ritchie (1993)
53.3	1.2	Ar–Ar	Orthoclase	Granite	54.2	−6	Thompson *et al.* (1987)
53.4	3.9	Ar–Ar	Whole rock	Ankaramitic basalt lava	73.2	−21	Upton *et al.* (1995)
53.5	1.8	K–Ar	Whole rock	Lamprophyre dyke	68.2	−28.5	Noble *et al.* (1988)
53.5	0.8	Rb–Sr	Mixed	Felsite	57.22	−6.2	Dickin (1981)
53.6	0.3	Ar–Ar	Plagioclase	Basaltic dyke	69.64	−54.8	Storey *et al.* (1998)
53.6	2	K–Ar	Whole rock	Dolerite	61.6	−1	Hitchen & Ritchie (1993)
53.7	2.2	K–Ar	Whole rock	Dyke	68.2	−28.5	Noble *et al.* (1988)
53.8	2.4	K–Ar	Whole rock	Alkaline basalt	69	−31	Noble *et al.* (1988)
53.8	2.2	K–Ar	Amphibole	Dyke	68.3	−28.3	Noble *et al.* (1988)
53.8	2.4	K–Ar	Whole rock	Alkaline basalt	69	−31	Noble *et al.* (1988)
54.1	1.4	K–Ar	Whole rock	Dolerite sill	61.6	−0.7	Hitchen & Ritchie (1993)
54.1	2.8	K–Ar	Whole rock	Alkaline basalt	69	−31	Noble *et al.* (1988)
54.3	0.5	Ar–Ar	Whole rock	Tuff glass	67	2	Sinton *et al.* (1998)
54.4	1.4	K–Ar	Whole rock	Basalt	58.2	−8.1	Hitchen & Ritchie (1993)
54.5	0.7	Ar–Ar	Whole rock	Tholeiitic sill	72.7	−22	Price *et al.* (1997)
54.6	3.4	FT	Zircon	Granophyre	54.3	−6	Brooks & Gleadow (1977)
54.8	2.4	K–Ar	Amphibole	Dyke	68.3	−28.3	Noble *et al.* (1988)
54.8	0.4	Ar–Ar	Plagioclase	Basaltic dyke	70.37	−53.5	Storey *et al.* (1998)
54.9	6.8	K–Ar	Whole rock	Tholeiitic basalt	68	−30	Noble *et al.* (1988)
54.9	1.2	Ar–Ar	Biotite	Granite	54.2	−6	Thompson *et al.* (1987)
54.9	1	Ar–Ar	Whole rock	Dacite	59.7	−9	Sinton *et al.* (1998)
55	1.6	Ar–Ar	Whole rock	Basalt	54.3	−6	Thompson *et al.* (1987)
55.2	2.8	Ar–Ar	Whole rock	Basalt	63	−40	Tegner & Duncan (1999)
55.3	0.8	Shrimp	Zircon	Granite	54.2	−6	Gamble *et al.* (1999)
55.3	1.4	K–Ar	Whole rock	Dolerite sill	61.6	−0.7	Hitchen & Ritchie (1993)
55.4	1.4	Ar–Ar	Whole rock	Basalt	63	−40	Tegner & Duncan (1999)
55.4	0.7	Ar–Ar	Biotite	Granophyre	68.2	−31.7	Hirschmann *et al.* (1997)
55.5	0.8	Ar–Ar	Amphibole	Granophyre	68.2	−31.7	Hirschmann *et al.* (1997)
55.5	4.4	Ar–Ar	Whole rock	Basalt	63	−40	Tegner & Duncan (1999)
55.6	2.4	K–Ar	Whole rock	Alkaline basalt	69	−31	Noble *et al.* (1988)
55.7	1	Rb–Sr	Whole rock	Granite	54.2	−6	Gibson *et al.* 1987)
55.7	1.8	K–Ar	Whole rock	Olivine nephelinite	63.7	7.7	Bugge *et al.* (1980)
55.8	1.4	K–Ar	Whole rock	Basalt	58.2	−8.1	Hitchen & Ritchie (1993)
55.8	1.8	Ar–Ar	Plagioclase	Basalt	58.5	−7.9	Sinton *et al.* (1998)
55.9	0.4	Rb–Sr	Whole rock	Granite	54.2	−6	Gibson *et al.* (1988)
56	1.3	Rb–Sr	Whole rock	Granite	54.2	−6	Gibson *et al.* (1988)
56	5.4	Ar–Ar	Whole rock	Basalt	56.5	−20	Sinton & Duncan (1998)
56	1.8	Ar–Ar	Whole rock	Basalt	63	−40	Tegner & Duncan (1999)
56	0.8	Ar–Ar	Plagioclase	Diabase sill	68.35	−32	Tegner *et al.* (1998)
56.1	5.8	Ar–Ar	Plagioclase	Basalt	63	−40	Tegner & Duncan (1999)
56.2	2.6	Ar–Ar	Whole rock	Basalt	63	−40	Tegner & Duncan (1999)
56.2	1.2	Ar–Ar	Whole rock	Dolerite dyke	66.4	−34.5	Tegner *et al.* (1998)
56.3	1.8	Ar–Ar	Whole rock	Diabase sill	68.12	−32	Tegner *et al.* (1998)
56.4	1.4	Shrimp	Zircon	Granite	54.2	−6	Gamble *et al.* (1999)
56.5	1.3	Shrimp	Zircon	Granophyre	54.2	−6.5	Gamble *et al.* (1999)

Age	$\pm 2\sigma$	Method	Mineral	Rock Type	Lat.	Long.	Author
56.5	2	Ar–Ar	Whole rock	Felsite intrusive	56.48	−6	Mussett (1986)
56.6	1.9	Ar–Ar	Whole rock	Dolerite	73.2	−21	Upton *et al.* (1995)
56.7	7	Ar–Ar	Whole rock	Dolerite	73.2	−21	Upton *et al.* (1995)
57	1.6	Ar–Ar	Whole rock	Granophyre	56.49	−6	Mussett (1986)
57.1	2.8	Ar–Ar	Whole rock	Basalt	63	−40	Tegner & Duncan (1999)
57.1	7.6	Ar–Ar	Whole rock	Basalt	63	−40	Tegner & Duncan (1999)
57.2	1.6	K–Ar	Whole rock	Dolerite sill	57.7	−6.9	Hitchen & Ritchie (1993)
57.5	2.2	Ar–Ar	Whole rock	Basalt lava	56.5	−5.5	Mussett (1986)
57.6	1.6	K–Ar	Whole rock	Dolerite sill	57.7	−6.9	Hitchen & Ritchie (1993)
58.1	3.2	Ar–Ar	Whole rock	Granophyre	56.41	−5.9	Mussett (1986)
58.4	2.8	K–Ar	Whole rock	Alkaline basalt	69	−31	Noble *et al.* (1988)
58.4	2.8	K–Ar	Whole rock	Alkaline basalt	68.5	−34	Noble *et al.* (1988)
58.4	0.8	Ar–Ar	Whole rock	Granophyre	57	−6.4	Mussett (1984)
58.4	0.7	Shrimp	Zircon	Porphyritic obsidian	54.7	−6.1	Gamble *et al.* (1999)
58.7	1.4	Ar–Ar	Whole rock	Nephelinite lava	73.2	−21	Upton *et al.* (1995)
58.7	1.7	Rb–Sr	Whole rock	Epigranite	57.22	−6.2	Dickin (1981)
59.3	1.4	Rb–Sr	K-Feldspar	Granophyre	57.2	−6.2	Dickin (1981)
59.4	1.8	Ar–Ar	Whole rock	Basalt lava	56.49	−5.95	Mussett (1986)
59.4	2.4	Ar–Ar	Whole rock	Basalt	63.5	−39.8	Sinton & Duncan (1998)
59.4	0.5	Ar–Ar	Plagioclase	Basaltic lava	70.5	−52.4	Storey *et al.* (1998)
59.7	3.2	Ar–Ar	Whole rock	Basalt lava	56.4	−6.05	Mussett (1986)
59.8	2.2	K–Ar	Whole rock	Basalt clast in conglom.	57.6	−7	Hitchen & Ritchie (1993)
60.1	3.4	K–Ar	Whole rock	Alkaline basalt	69	−31	Noble *et al.* (1988)
60.1	1	Ar–Ar	Whole rock	Basaltic lava	57	−6.4	Mussett (1984)
60.3	1.6	Ar–Ar	Plagioclase	Basalt	63.5	−39.8	Sinton & Duncan (1998)
60.3	4.2	Ar–Ar	Whole rock	Basalt	63.5	−39.8	Sinton & Duncan (1998)
60.3	0.4	Ar–Ar	Plagioclase	Basaltic lava	69.6	−53	Storey *et al.* (1998)
60.3	1	Ar–Ar	Whole rock	Hyaloclastite glass	70.19	−53.4	Storey *et al.* (1998)
60.4	0.5	Ar–Ar	Whole rock	Picritic lava	70.66	−53.8	Storey *et al.* (1998)
60.5	0.4	Ar–Ar	Plagioclase	Basaltic lava	70.27	−52.6	Storey *et al.* (1998)
60.7	0.5	Ar–Ar	Whole rock	Hyaloclastite glass	70.07	−53.5	Storey *et al.* (1998)
60.7	2.8	K–Ar	Whole rock	Basalt	58.5	−7.6	Hitchen & Ritchie (1993)
60.8	2.8	Ar–Ar	Whole rock	Basalt lava	56.5	−6.05	Mussett (1986)
61	1.2	Ar–Ar	Whole rock	Dacite	63.5	−39.8	Sinton & Duncan (1998)
61.1	2.8	Ar–Ar	Whole rock	Basalt lava	56.5	−6	Mussett (1986)
61.4	2	K–Ar	Whole rock	Basalt	59.2	−10.2	Hitchen & Ritchie (1993)
61.9	2.6	K–Ar	Whole rock	Basalt clast in conglom.	57.6	−7	Hitchen & Ritchie (1993)
61.9	2.2	K–Ar	Whole rock	Basalt	59.2	−10.2	Hitchen & Ritchie (1993)
62.3	1.4	Ar–Ar	Plagioclase	Tuff	63.5	−39.8	Sinton & Duncan (1998)
62.3	0.6	Ar–Ar	K-Feldspar	Tuff	56.7	−6.3	Pearson *et al.* (1996)
62.4	2.6	K–Ar	Whole rock	Basalt	58.5	−7.6	Hitchen & Ritchie (1993)
62.8	0.6	Ar–Ar	Sanidine	Tuff	56.7	−6.3	Pearson *et al.* (1996)
63.3	1	Ar–Ar	Whole rock	Basalt	63.5	−39.8	Sinton & Duncan (1998)
63.3	1.2	Ar–Ar	Whole rock	Basalt	63.5	−39.8	Sinton & Duncan (1998)